

MULTI-SPACECRAFT OBSERVATIONS OF RECURRENT <sup>3</sup>HE-RICH SOLAR ENERGETIC PARTICLES

R. BUČÍK AND D. E. INNES AND U. MALL AND A. KORTH

Max-Planck-Institut für Sonnensystemforschung, D-37191 Katlenburg-Lindau<sup>1</sup>, Germany

G. M. MASON

Applied Physics Laboratory, Johns Hopkins University, Laurel, MD 20723, USA

AND

R. GÓMEZ-HERRERO

Space Research Group, University of Alcalá, E-28871 Alcalá de Henares, Spain

*Draft version March 20, 2014*

## ABSTRACT

We study the origin of <sup>3</sup>He-rich solar energetic particles ( $<1$  MeV nucleon<sup>-1</sup>) that are observed consecutively on *STEREO-B*, *ACE*, and *STEREO-A* spacecraft when they are separated in heliolongitude by more than 90°. The <sup>3</sup>He-rich period on *STEREO-B* and *STEREO-A* commences on 2011 July 1 and 2011 July 16, respectively. The *ACE* <sup>3</sup>He-rich period consists of two sub-events starting on 2011 July 7 and 2011 July 9. We associate the *STEREO-B* July 1 and *ACE* July 7 <sup>3</sup>He-rich events with the same sizeable active region producing X-ray flares accompanied by prompt electron events, when it was near the west solar limb as seen from the respective spacecraft. The *ACE* July 9 and *STEREO-A* July 16 events were dispersionless with enormous <sup>3</sup>He enrichment, lacking solar energetic electrons and occurring in corotating interaction regions. We associate these events with a small, recently emerged active region near the border of a low-latitude coronal hole that produced numerous jet-like emissions temporally correlated with type III radio bursts. For the first time we present observations of 1) solar regions with long-lasting conditions for <sup>3</sup>He acceleration and 2) solar energetic <sup>3</sup>He that is temporary confined/re-accelerated in interplanetary space.

*Subject headings:* interplanetary medium — solar wind — Sun: flares — Sun: particle emission

## 1. INTRODUCTION

Solar energetic particle (SEP) <sup>3</sup>He-rich events are characterized by huge abundance enhancements of the rare isotope <sup>3</sup>He (up to factors of  $>10^4$ ) over solar system abundances. The enrichment of the <sup>3</sup>He is believed to be caused by selective heating due to wave-particle interaction in the flare plasma because of its unique charge to mass ratio (see e.g., reviews by Kocharov & Kocharov 1984; Reames 1990). Earlier studies have shown that <sup>3</sup>He-rich SEP events are associated with 2-100 keV electron events (Reames et al. 1985) and their related type III radio bursts (Reames & Stone 1986), which are excited by electrons streaming outward through interplanetary space (e.g., Lin 1974). The events have been associated with minor soft X-ray flares (e.g., Zwickl et al. 1978; Kahler et al. 1987; Reames et al. 1988). Recently the sources of <sup>3</sup>He-rich events have been investigated using extreme ultraviolet (EUV) and X-ray solar images (Nitta et al. 2006, 2008; Wang et al. 2006). The responsible source has often been attributed to a jet-like ejection near a coronal hole.

Sequences of <sup>3</sup>He-rich SEP events from the same active region (AR) have been observed with a single spacecraft (s/c) (Reames & Stone 1986; Mason et al. 1999, 2000; Wang et al. 2006; Pick et al. 2006) only in a limited time interval (about one day) presumably due to loss of the magnetic connection to the flare site. These recurrent

events may suggest almost continuous acceleration of <sup>3</sup>He in the single AR (Pick et al. 2006). In addition, multi-day periods of solar energetic <sup>3</sup>He have been recently discovered with the *Advanced Composition Explorer* (*ACE*) often with no individual <sup>3</sup>He-rich events resolved (Mason 2007, and references therein). Such long periods have been interpreted as a combination of continuous production of <sup>3</sup>He-rich SEPs and their confinement in interplanetary magnetic field structures (Kocharov et al. 2008).

In this paper we report, for the first time, on a <sup>3</sup>He-rich period of SEPs consecutively observed by three widely, in longitude, separated spacecraft *STEREO-B*, *ACE* and *STEREO-A* with delays corresponding to the Carrington rotation rate. The ultimate goal of this study is to identify activity on the Sun and the conditions in interplanetary space leading to the long persistence of energetic <sup>3</sup>He in the heliosphere. In Section 2, we describe energetic particle and solar wind plasma observations on each s/c. The responsible solar sources are identified in Section 3 using a combination of coronal field model extrapolations, EUV and radio observations. The results are summarized and discussed in Section 4.

## 2. ENERGETIC PARTICLE OBSERVATIONS

The helium isotope observations described in this paper are from the time-of-flight mass spectrometers Suprathermal Ion Telescope (SIT; Mason et al. 2008) on the two *Solar Terrestrial Relations Observatories* (*STEREO*) and Ultra Low Energy Isotope Spectrometer (ULEIS; Mason et al. 1998) on *ACE*. The instru-

bucik@mps.mpg.de

<sup>1</sup> since 2014 February: D-37077 Göttingen

ments have sunward viewing directions close to the average Parker magnetic field spiral line (*STEREO*) or in the sunward hemisphere (*ACE*). They measure ions from He to Fe in the energy range from 20 keV nucleon<sup>-1</sup> to several MeV nucleon<sup>-1</sup>. Both *STEREO* s/c are in a heliocentric orbit at  $\sim 1$  AU near the ecliptic plane increasing their separation from Earth at a rate of  $\sim 22^\circ$  per year. *STEREO-A* is preceding Earth and *STEREO-B* is trailing behind. The *ACE* s/c is in an orbit around the L1 Lagrangian point,  $\sim 0.01$  AU upstream of Earth in the sunward direction. During the <sup>3</sup>He-rich period investigated in this paper *STEREO-B* was  $93^\circ$  behind and *STEREO-A*  $99^\circ$  ahead of the Earth with the heliocentric distances of 1.02 and 0.96 AU, respectively. These angular separations correspond to corotation delays of 7.1 and 7.5 days, respectively, using the Carrington rotation period of 27.3 days.

Since the magnetic connection of the spacecraft to the Sun lies west of the central meridian viewed by each spacecraft, the *GOES* spacecraft at Earth was able to observe source regions for *STEREO-B* as well as *ACE*, but not for *STEREO-A*.

### 2.1. *STEREO-B* <sup>3</sup>He-Rich Period

Figure 1 presents energetic particle and solar wind plasma measurements for the <sup>3</sup>He-rich period starting on 2011 July 1 on *STEREO-B*. Figure 1a shows *STEREO-B* 10-min electron intensities from the STE-D (Lin et al. 2008) anti-sunward pointing detector and from the SEPT (Müller-Mellin et al. 2008) sunward pointing sensor centered on the nominal Parker spiral direction. The data from the sunward pointing STE-U are not available, because the instrument is saturated by sunlight (Wang et al. 2012). A solar energetic electron event was clearly observed on 2011 July 1 with an onset at  $\sim 13:10$  UT and a velocity dispersion down to 3 keV. At higher energies ( $>100$  keV) increases in the electron intensity were not detected by SEPT. The event was associated with B4.1 *GOES* X-ray flare in the 1-8 Å range and H $\alpha$  flare with a start time at 12:34 UT. According to the Edited Solar Events Lists<sup>2</sup> compiled by the NOAA Space Weather Prediction Center (SWPC) the flare originated from AR 11244 (N15°W05° as viewed from Earth) and was accompanied by a type III radio burst. From the *STEREO-B* point of view the AR was located at  $\sim W97^\circ$ .

The period of <sup>3</sup>He-rich SEPs on 2011 July 1 shows quite low ion increases. Figure 1b shows the SIT mass spectrogram of all individual ions in the energy ranges 0.25-0.90 MeV nucleon<sup>-1</sup> (mass  $<8$  amu) and 0.08-0.15 MeV nucleon<sup>-1</sup> (mass  $>8$  amu). The spectrogram indicates that the number density of the ions started to increase roughly around 21 UT. Taking the lower energy limit of the ions in Figure 1b the estimated injection on the Sun would be at 14 UT. The 1-hr SEPT ion intensities in Figure 1c show only a minor (factor of  $\sim 3$ ) enhancement above the background. Observations in Figure 1b show that the SIT pulse-height points are spread over the whole helium mass range. To rule out <sup>4</sup>He spillover to the <sup>3</sup>He we compare in Figure 2 helium SIT-B histograms for the 2011 July 1 period and a typical corotating interaction region (CIR) event, which

is almost all <sup>4</sup>He. The figure clearly indicates a separate <sup>3</sup>He peak in the valley of the CIR histogram. The <sup>3</sup>He/<sup>4</sup>He elemental ratio was determined by summing the counts in the two clearly separated He isotope peaks in the mass histogram. Note that at higher energies the *STEREO-B*/LET (Mewaldt et al. 2008) instrument shows no <sup>3</sup>He increase on July 1-2 in the He mass spectrogram plots in intervals 2.3-3.3, 4.3-8.0 MeV nucleon<sup>-1</sup>. The 385 keV nucleon<sup>-1</sup> <sup>3</sup>He/<sup>4</sup>He and Fe/O abundance ratios for the <sup>3</sup>He-rich period in this study on all three spacecraft are listed in Table 1. The table further shows s/c Carrington longitudes and heliographic latitudes, the start and end times of the period on the different spacecraft, and the <sup>3</sup>He fluences.

Figure 1d shows 10-min averages of solar wind speed  $V$  and the total pressure  $P$ , which is given by the sum of the thermal and magnetic pressure, i.e.,  $P \sim n_p k(1.16T_p + 1.3 \times 10^5) + B^2/2\mu_0$ , where  $n_p$  and  $T_p$  are the proton density and temperature, respectively, and  $B$  is the magnetic field magnitude. The thermal pressure, taken from Jian et al. (2006), includes the contribution of solar wind electrons and alpha particles. Solar wind proton and magnetic field data were obtained from the PLASTIC (Galvin et al. 2008) and MAG (Acuña et al. 2008) instruments on *STEREO*. The total pressure shows no increase over the ambient solar wind pressure. The onset of a high-speed solar wind on 2011 July 2 was preceded by the magnetic field polarity reversal. IMF (interplanetary magnetic field) polarity color bar in Figure 1 indicates in red (green) the times when the observed magnetic field vector was oriented toward (away from) the Sun. The polarity sectors are defined as  $\pm 70^\circ$  about the nominal Parker angle. The Parker angle was calculated using the observed solar wind speed. The yellow indicates when the magnetic field vector was within the range  $\pm 20^\circ$  about the normal to the nominal Parker magnetic field direction.

### 2.2. *ACE* <sup>3</sup>He-Rich Period

Figure 3 presents energetic particle and solar wind plasma parameters throughout the *ACE* <sup>3</sup>He-rich period starting on 2011 July 7 and terminating at the end of 2011 July 10. Figure 3a shows 5-min energetic electron intensities. The near-relativistic electrons are routinely monitored on *ACE*, but because of the data gap between 05 and 11 UT on July 8 the intensities are shown from the WIND/3DP (Lin et al. 1995), located also near the L1 point. The measurements in Figure 3a clearly show four impulsive solar energetic electron events with onset times at  $\sim 05:50$ , 14:50, 20:55 UT on 2011 July 7 and 03:20 UT on 2011 July 8 at 182 keV. On shorter time scales, velocity dispersion is evident in all these electron events. The events were associated with B2.6, B7.6, B6.4, B3.0 X-ray flares with start times at 05:09, 14:25, 20:24 UT on July 7 and at 02:53 UT on July 8, respectively. According to the NOAA SWPC list the B2.6 and B3.0 flares originated from AR 11244 (N15°W82°) and AR 11243 (N16°W60°), respectively. On 2011 July 7 both solar regions were associated with sunspots; AR 11243 contained several bipolar sunspots and AR 11244 only one visible unipolar sunspot as reported in the NOAA Solar Region Summary (SRS). The B7.6 and B6.4 flares do not have an assigned solar region in the event list. All these four

<sup>2</sup> www.swpc.noaa.gov

flares were accompanied by type III solar radio bursts detected by different ground-based observatories, as reported in the NOAA list. No related H $\alpha$  flare is recorded in the H-Alpha Solar Flare Report at the NOAA National Geophysical Data Center<sup>3</sup>. The arrow in Figure 3a indicates the time of the EUV jet on July 8 (16:25 UT) identified in the next section (Section 3.2.3).

The 1-hr 0.23-0.32 MeV nucleon<sup>-1</sup>  $^3\text{He}$  intensity in Figure 3b shows two separate events or sub-periods, one starting near the end of 2011 July 7 ( $\sim$ 21:00 UT) and another at the beginning of 2011 July 9 ( $\sim$ 01:00 UT). Two double-ended arrows in Figure 3b denote the *STEREO-B* and *STEREO-A*  $^3\text{He}$ -rich periods (as in Table 1) shifted in corotation time. The partial overlap of the periods on all three s/c suggests a common solar origin. Due to its smaller geometrical factor, the SIT instrument is less sensitive to the weak  $^3\text{He}$ -rich events than the ULEIS. Thus the  $^3\text{He}$ -rich periods observed by ULEIS have generally longer duration. The high energy (0.4-10 MeV nucleon<sup>-1</sup>) mass spectrogram data (Figure 3c) show that the first  $^3\text{He}$  ions arrived around 12:00 UT on 2011 July 7. These are likely to be related to the first electron event seen on the same day. The 2011 July 7  $^3\text{He}$ -rich event itself may have come from multiple injections. The beginning of this period was probably associated with the second electron event. The estimated delay between 100 keV electrons and 0.23-0.32 MeV nucleon<sup>-1</sup> ions traveling along the same path length from the Sun to L1 would be  $\sim$ 6.5 hours, which approximately agrees with the observed time offset. There is a small additional  $^3\text{He}$  intensity increase observed at the beginning of 2011 July 8 followed by increases in the heavy-ion (Fe and O) intensities (see Figure 3b). This increase could be related to the most intense electron event seen at the end of 2011 July 7. It is not clear if any  $^3\text{He}$  was associated with the solar electron event at the beginning of July 8. The presence of an enhanced  $^3\text{He}$  intensity from the previous activity along with a data gap at 05-11 UT would obscure any  $^3\text{He}$  injection associated with this electron event. There were no observed electron increases closely preceding the 2011 July 9  $^3\text{He}$ -rich event. A small dispersed electron event at energy  $<10$  keV is seen on July 9 after the SEP event start time. From Figure 3b we can see that the July 9 event is more enriched in  $^3\text{He}$  and also shows higher  $^3\text{He}$  intensities compared to the event on July 7. The Fe and O time lines lie nearly on top of each other for both events. The abundance ratios for these two *ACE* events are listed in Table 1. The time intervals used for calculating the ratios and fluences are only approximate and roughly coincide with the enhanced Fe/O ratio. The *ACE*/SIS (Stone et al. 1998) instrument in the energy intervals 4.5-7.6, 7.6-16.3 MeV nucleon<sup>-1</sup> shows a high  $^3\text{He}/^4\text{He}$  ratio ( $\sim$ 0.5-1.0) for the July 7 period in the spectrogram plots at the ACE science center<sup>4</sup>. On July 9 the  $^3\text{He}$  in these high energy ranges is only seen during 00-06 UT. It was probably a continuation from previous day and related to the July 7 event. Figure 3d shows 1-hr *ACE*/EPAM (Gold et al. 1998) ion intensities at 120° from the sunward pointing axis. The data from the telescope looking towards the Sun (LEMS30) are not

available for energies  $<1$  MeV. The intensity-time profiles in Figure 3d indicate a velocity dispersion at the onset of the July 7 event and a dispersionless onset for the July 9 event.

The IMF polarity color bar in Figure 3 indicates that the two  $^3\text{He}$ -rich events occurred in opposite magnetic polarity sectors. In addition, the intensity plots in Figures 3b and 3d show that the end of July 7 event and the start of July 9 event coincide with the interplanetary magnetic sector boundary crossing. The solar wind data in Figure 3e reveal a CIR on July 9, characterized by a gradual solar wind speed rise and the pressure enhancement. Because of the data gap on *ACE* the proton plasma density used in the total pressure is from the *WIND*/SWE (Ogilvie et al. 1995) instrument. The remaining solar wind parameters are from MAG (Smith et al. 1998) and SWEPA (McComas et al. 1998) on *ACE*. CIRs arise when fast solar wind, emerging from coronal holes, overtakes the preceding slow solar wind. The leading and trailing edge of the interaction region are characterized by an increase and decrease in the total pressure, respectively, and the enhanced pressure occurs in the rising part of the speed profile (e.g., Burlaga 1995). There is a gradual change in the flow direction from near radial to the east (refer to Figure 3f) at the beginning of July 9, which is synchronized with the start of the slow rise in the solar wind speed. Although the boundary between the two solar wind regimes here is not sharp, such a transition can indicate an evolving stream interface. Apart from pure time evolution the s/c heliographic latitude could also be playing some role in the observed high-speed stream structure. We notice from Figure 3 that the July 9  $^3\text{He}$ -rich event commenced before the interface, and close to the time that the change of the magnetic polarity occurred. It is interesting that the period of relatively enhanced  $^3\text{He}$  on July 10 coincides with large variations in the high-speed solar wind and further deflection of the flow toward the east.

### 2.3. *STEREO-A* $^3\text{He}$ -Rich Period

#### 2.3.1. General Properties

The  $^3\text{He}$ -rich period of interest starts for *STEREO-A* on 2011 July 16. The simultaneous energetic particle and solar wind plasma measurements during the  $^3\text{He}$ -rich period on *STEREO-A* are presented in Figure 4. Figure 4a shows 10-min electron intensities from the STE-D anti-sunward and the SEPT sunward pointing sensors. No obvious solar electron event is seen in the presented time range. On 2011 July 16 the electron intensities were near background level. The STE electron intensities at higher energies were dominated by energetic ions (see Wang et al. (2012) for a description of the background in STE). Arrows in Figure 4a denote EUV brightenings (12:40, 14:15, 18:45 UT) and a jet (22:25 UT) on July 15 identified in the next section (Section 3.2.4). A marked  $^3\text{He}$  enhancement is seen in the SIT mass spectrogram in Figure 4b. There is a data gap on July 16 from 09:45 to 11:57 UT in the SIT measurements at the beginning of the  $^3\text{He}$ -rich period. Therefore we plot in Figure 4c 1-hr ion intensities between 0.18 and 1.49 MeV from the SEPT sunward sensor which did not suffer from this data gap. The onset at  $\sim$ 09:30 UT is clearly disper-

<sup>3</sup> [www.ngdc.noaa.gov](http://www.ngdc.noaa.gov)

<sup>4</sup> [www.srl.caltech.edu/ACE/ASC/DATA/level3/sis/heplots/](http://www.srl.caltech.edu/ACE/ASC/DATA/level3/sis/heplots/)

sionless with a simultaneous rise of ion intensities in all energy channels. Note that the approximate delay time between ions in the lowest and highest energy channels in Figure 4c would be at least 5 hours. This estimate is based on scatter-free ion propagation (with zero pitch angle) along the spiral with a path length of 1.1 AU to *STEREO-A*, assuming a solar wind speed of  $400 \text{ km s}^{-1}$ . Dispersionless onset indicates that the first solar energetic particles arrived to 1 AU before the s/c enters the flare connected field lines (Kocharov et al. 2008). This could also be the reason for the lack of electron enhancement. Dispersionless  $^3\text{He}$ -rich events associated with interplanetary shocks or magnetic clouds were reported by Tsurutani et al. (2002). The SEPT ion enhancements shown in Figure 4c are relatively minor and comparable with the pre-event intensities. The statistical errors of SEPT ion intensities during the  $^3\text{He}$ -rich period are low and therefore not shown. For instance, the errors range between 0.1 and 0.3 in the highest energy channel. The second (lower) black curve in Figure 4c shows the 1.49 MeV ion intensity from the SEPT anti-sunward pointing detector. The energetic ion fluxes appear to be only slightly anisotropic with intensities in the sunward pointing detector higher by about a factor of  $\sim 2$ . Similar small anisotropies were seen in the lower energy channels. The  $^3\text{He}$ -rich events usually exhibit large (outward to sunward ratio  $>10$ ) and long lasting anisotropies (e.g., Zwickl et al. 1978). We remark that SEPT is not capable of elemental resolution and most of the time protons are the contributors in the ion channels. However, for a  $^3\text{He}$ -rich SEP event, helium can account for a sizable amount (Müller-Mellin et al. 2008). The elemental abundances for 2011 July 16  $^3\text{He}$ -rich event have been examined in an earlier report by Bučík et al. (2013b). This study shows that heavy ions are also enriched in this event with the relative abundances of elements (Ne-S) and Fe typical of  $^3\text{He}$ -rich SEP events (e.g., Mason et al. 2004). The 385 keV nucleon $^{-1}$   $^3\text{He}/^4\text{He}$  and Fe/O ratios for this event are in Table 1. The *STEREO-A*/LET instrument shows a clear  $^3\text{He}$  increase for the July 16 event in the energy interval 2.3-3.3 MeV nucleon $^{-1}$  with a high  $^3\text{He}/^4\text{He}$  ratio ( $>1$ ) but not in 4.3-8.0 MeV nucleon $^{-1}$ .

Figure 4d shows 10-min averages of solar wind speed  $V$  and total pressure  $P$ . The shaded region marks the time interval of a CIR obtained from a list<sup>5</sup> compiled by the *STEREO* magnetometer team at the University of California Los Angeles (UCLA), based on plasma and magnetic field data (Jian et al. 2006). Note that the total pressure  $P$  peak is a factor of  $\sim 2$  higher than in the CIR on 2011 July 9. We see in Figure 4d that the CIR trailing boundary is well-defined with a jump-like decrease (increase) in the pressure  $P$  (speed  $V$ ), suggestive of a developing reverse shock. The dashed vertical line indicates the stream interface (SI), separating slow and fast stream plasma, characterized by a sharp discontinuity in the azimuthal flow direction (Figure 4e) and a jump in the flow speed (Figure 4d) (Gosling et al. 1978). Other characteristics of the stream interface such as abrupt and simultaneous drops in plasma proton density and rise in proton temperature were also observed. A more detailed investigation of the solar wind plasma

data revealed a smooth North to South rotation of the magnetic field vector over  $120^\circ$  during a relatively short time period ( $\sim 4$  hr) around the peak of the total pressure. This feature together with a strong magnetic field (up to  $\sim 20$  nT) and local decrease in  $n_p$  tentatively suggests the presence of a magnetic cloud embedded within the CIR. However other essential characteristics of a magnetic cloud, such as abnormal  $T_p$  depression (Richardson & Cane 1995) and bidirectional beams of suprathermal ( $\sim 100$  eV) electrons (Gosling & McComas 1987) were not observed. The pitch angle distribution of suprathermal electrons on *STEREO* was examined in data<sup>6</sup> from the SWEA instrument (Sauvaud et al. 2008). Moreover, the magnetic field rotation occurred near the sector boundary crossing and thus may be related to the complex magnetic morphology in the heliospheric current sheet (Klein & Burlaga 1980). Note that the purported magnetic cloud is not included in the comprehensive list of the *STEREO* interplanetary coronal mass ejections compiled by the previously cited team at UCLA. Recently, Gómez-Herrero et al. (2011) presented several cases of similar cloud-like small structures embedded within the CIR which probably favored the formation of reverse shocks, resulting in enhanced ion acceleration.

### 2.3.2. Association with the CIR

The observations in Figure 4 indicate that ion intensities and  $^3\text{He}$  counts on July 16 commence to increase near the stream interface and show a maximum in the vicinity of the CIR trailing edge. Such ion intensity increases are commonly observed in ion intensity-time profiles in CIR events at 1 AU (e.g., Richardson & Zwickl 1984; Mason et al. 1997; Chottoo et al. 2000). We emphasize here that the ion intensities tend to peak simultaneously at all energies. Particularly, the low energy channels show a pronounced peak at the trailing boundary which indicates that the energy spectrum was locally modified. In the standard basic picture of CIR acceleration, particles can be pre-heated inside the compression region (e.g., by a stochastic mechanism) and then accelerated in the reverse shock formed at the CIR trailing boundary. The stream interface is usually assumed to be a tangential discontinuity through which particle transport is not expected to occur. Therefore the ion intensity decreases towards the interface in the CIRs (Crooker et al. 1999, and references therein). Weak, sunward streaming of ions with energy  $>1$  MeV nucleon $^{-1}$  has been reported in CIR events at 1 AU (Richardson et al. 1993), indicating their source is in the outer heliosphere, while low energy ions ( $<300$  keV) showed anti-sunward streaming in the compressed solar wind inside CIRs (Richardson & Zwickl 1984).

We can see in Figure 4d that the high speed solar wind is quite variable behind the interface. An interesting feature of the high speed wind in the middle of July 17 is the weaker helium enhancement, mainly seen in the  $^4\text{He}$  isotope. The enhancement commences when there is a sharp drop in the speed and another deflection of the flow toward the east, while the pressure stays at the background level. This has similarities to the L1 observations on July 10 in the high-speed solar wind.

<sup>5</sup> [www-ssc.igpp.ucla.edu/forms/stereo/stereo\\_level\\_3.html](http://www-ssc.igpp.ucla.edu/forms/stereo/stereo_level_3.html)

<sup>6</sup> [stereo.cesr.fr/plots.php](http://stereo.cesr.fr/plots.php)

$^4\text{He}$  intensity variations coincident with increases or decreases in solar wind speed have been previously noticed by Mason et al. (2009) in the CIR events. The variations have been attributed to the changes in connection of the spacecraft to different locations in the CIR outside 1 AU. We find that the  $137\text{ keV nucleon}^{-1}\text{ Fe/O}$  abundance ratio is  $0.20 \pm 0.07$  during the helium enhancement on July 17 between 08 and 16 UT. Note that statistically significant Fe/O ratios at higher energies were not available in this time interval. While the helium isotope ratio ( $^3\text{He}/^4\text{He}$ ) remains enhanced during this interval (as implied by the mass spectrogram) the Fe/O is smaller than the typical ratio in  $^3\text{He}$ -rich events ( $\sim 0.95$  at  $385\text{ keV nucleon}^{-1}$  in Mason et al. 2004), but somewhat above the value typical for CIR events ( $\sim 0.08$  at  $150\text{ keV nucleon}^{-1}$  in Mason et al. 1997) or ( $\sim 0.10$  at  $137\text{ keV nucleon}^{-1}$  in Bučík et al. 2012) suggesting that a mixed population co-existed during this time interval in the high-speed solar wind.

Further, Figure 4b shows a brief  $^4\text{He}$  increase at the beginning of July 16 which occurred inside the compression region preceding the stream interface. Ion intensity enhancements in this part of CIRs have been related to the CIR forward shock acceleration (Barnes & Simpson 1976). The enhancements were less intense or even not present at 1 AU with larger H/He ratio ( $\sim 43$ ) (Richardson et al. 1993) than that associated with the CIR trailing edge (e.g.,  $\sim 12.5$  at  $386\text{ keV nucleon}^{-1}$  in the survey of Bučík et al. 2012). The  $386\text{ keV nucleon}^{-1}$  H/He ratio integrated through this  $^4\text{He}$  increase between 23 UT on July 15 and 04 UT on July 16 is  $45.4 \pm 8.1$  and it is strikingly similar to the H/He ratio reported by Richardson et al. (1993) for corotating increases in the slow solar wind. The heavy-ion count rates during this enhancement were weak with the Ne-S and Fe fluences statistically not significant (with errors greater than 0.5) in the SIT energy range.

### 3. SOLAR SOURCES

To determine the solar origin of the  $^3\text{He}$ -rich SEPs described in the previous section we identify the s/c magnetic connection location on the Sun and then examine flaring at this location using the EUV solar images. For the events which are associated with energetic electrons and X-ray flares the identification of the responsible solar source is more straightforward compared to the cases which lack such an association. In these situations we also use the radio data which generally show wider longitude coverage than their parent electrons. Nitta et al. (2006) have found a  $\sim 95\%$  association of  $\sim 2\text{--}3\text{ MeV nucleon}^{-1}$   $^3\text{He}$ -rich SEP events with type III bursts and only a  $\sim 62\%$  association with  $>30\text{ keV}$  solar electron events.

#### 3.1. Spacecraft Magnetic Connections

Figure 5 shows photospheric magnetic field maps with potential-field source-surface (PFSS) (Schatten et al. 1969) model coronal field lines at the start times of the *STEREO-B* 2011 July 1, *ACE* July 7 and July 9, and *STEREO-A* July 16  $^3\text{He}$ -rich events. Black and white areas indicate regions with strong magnetic fields of negative and positive polarity. The regions with predominantly one polarity correspond to coronal holes and the

bipolar areas to active regions. The field lines shown are those which are open to the heliosphere for the range of the s/c heliolatitudes. The PFSS extrapolations we use are based on *Solar Dynamic Observatory* Helioseismic and Magnetic Imager (*SDO/HMI*) magnetograms which are assimilated into the flux-dispersal model to provide the magnetic field on the full solar sphere (Schrijver & DeRosa 2003). These photospheric magnetic field maps with a temporal resolution of 6 hours are provided by Lockheed Martin Solar and Astrophysics Laboratory and are available via the Solar Soft PFSS package<sup>7</sup>. The black vertical lines in Figure 5 indicate the east (top panel) and west (remaining panels) solar limbs as viewed from the Earth. Blue diamonds mark the footpoints of *STEREO-B* (top panel), L1 (two middle panels) and *STEREO-A* (bottom panel) at the source surface at  $2.5 R_{\odot}$  from Sun center. The source surface is a boundary which separates open and closed fields. Outside the source surface we assume the field follows the Parker spiral. The s/c footpoint longitudes were determined from the Parker angle using the measured solar wind speed. Yellow circles indicate the s/c connection location on the Sun. The location on the Sun was identified by tracking the s/c footpoints over the  $^3\text{He}$ -rich period. The technique which combines the Parker spiral for the interplanetary space and the PFSS model for the corona has been previously used in identification of  $^3\text{He}$ -rich SEP events sources (e.g., Nitta et al. 2006; Wang et al. 2006). In this study we also check whether the in-situ magnetic field polarity matches the polarity from the PFSS extrapolations.

The top panel in Figure 5 shows that the *STEREO-B* footpoint at the start time of the 2011 July 1  $^3\text{He}$ -rich period was located near the positive (green) field lines of the low-latitude coronal hole and  $\sim 5^{\circ}\text{--}10^{\circ}$  away from the negative (red) field lines emanating from AR 11243 and AR 11244. It was pointed out that the footpoint longitude, based on a simple Parker spiral with a constant solar wind speed, can only be estimated within  $\pm 10^{\circ}$  (Nolte & Roelof 1973; Klein et al. 2008). The in-situ polarity (see Figure 1) suggests that the main connection was via negative field, although a few short excursions to the positive field near the beginning of the event are also present. Since the intersection points of the negative polarity field lines from the two ARs, 11243 and 11244, have equal distance to the *STEREO-B* footpoint, it is not possible to unambiguously determine the connection region on the Sun. The second panel in Figure 5 shows the L1 footpoint at the start time of 2011 July 7  $^3\text{He}$ -rich event was connected via negative (red) field lines to AR 11244. At that time the Earth was generally in the negative polarity sector with some deviations from the nominal Parker field direction as indicated by the yellow coding in the polarity color bar in Figure 3. One can see in the third panel of Figure 5 that at the start time of 2011 July 9 event the L1 footpoint on the source surface was between the positive (green) field lines of the low-latitude coronal hole (with nearby AR 11246) and negative (red) field lines of AR 11243. The in-situ polarity in Figure 3 suggests connection via positive field. The bottom panel in Figure 5 suggests that *STEREO-A* was connected to the same coronal hole during the 2011

<sup>7</sup> [www.lmsal.com/\\$\sim\\$derosa/pfsspack](http://www.lmsal.com/$\sim$derosa/pfsspack)

July 16  $^3\text{He}$ -rich period, in agreement with the in-situ polarity observations. The coronal hole was presumably the source of the high-speed solar wind responsible for the CIRs observed on July 9 by near-Earth s/c and on July 16 by *STEREO-A*. Furthermore, the sequence of the photospheric maps with a modeled coronal field showed that both July 9 and July 16  $^3\text{He}$ -rich periods terminated when the s/c lost the connection to the coronal hole.

### 3.2. EUV Observations

Below we examine data from the Sun Earth Connection Coronal and Heliospheric Investigation (SECCHI) EUV imager (EUVI; Howard et al. 2008) on *STEREO-A* and the Atmospheric Imaging Assembly (AIA; Lemen et al. 2012) on *SDO*. The *STEREO*/EUVI is taking full-Sun images with 5-minute regular cadence in four EUV wavelengths and *SDO*/AIA with an unprecedented 12-sec cadence in seven EUV wavelengths. Note that while *STEREO* is on a heliocentric orbit and increases its separation from the Earth, *SDO* is in orbit around the Earth

#### 3.2.1. *STEREO-B* 2011 July 1 Event

We have already shown that the 2011 July 1  $^3\text{He}$ -rich period was preceded by an electron event with energies below  $\sim 50$  keV. The source-surface model of the coronal field along with the in-situ polarity suggests connection to the both ARs 11243 and 11244. The associated X-ray and  $\text{H}\alpha$  flares are assigned to the AR 11244 in the NOAA/SWPC list, favoring this region as the most probable source candidate for the  $^3\text{He}$  event. This is further confirmed with the EUV solar images obtained from *SDO*/AIA. These images reveal eruptions of material into the corona from AR 11244 starting at  $\sim 12:20$  UT with marked brightening around the time of the X-ray flare, but no activity in AR 11243. Kahler et al. (1987) for instance associated the sources of  $^3\text{He}$ -rich events with filament eruptions. AR 11244 remained active for some time, producing for example several X-ray flares (mainly B class) on 2011 July 3, as reported in the NOAA list.

#### 3.2.2. *ACE* 2011 July 7 Event

The 2011 July 7  $^3\text{He}$ -rich event was associated with two solar electron events whose associated B7.6 and B6.4 X-ray flares were not assigned to an AR in the NOAA/SWPC list. Our suggested magnetic connection region on the Sun is AR 11244. As shown in Figure 5 (2011-Jul-7.9 panel) the region was near the west solar limb as seen from Earth. The flares might have been partly occulted and perhaps were stronger than measured.

Figure 6 shows the EUV 131 Å *SDO*/AIA four-minute difference images near the times of B7.6 (upper panel) and B6.4 (lower panel) flares on 2011 July 7. The displayed images are the difference of intensity two minutes after and two minutes before the X-ray flare start times. In both cases the brightening on the west limb was accompanied by eruptions of the material into the corona nicely visible in the 304 Å *SDO*/AIA channel. To be sure that the brightenings originated in AR 11244 we examined *STEREO-A*/SECCHI EUV images. In the *STEREO-A* field of view, AR 11244 was seen near the central meridian. The eruptions in the AR were, in both

cases, bright for about 20 minutes. The AIA EUV image in the 131 Å channel corresponds to  $\sim 0.4$  MK (Fe VIII) and to 10 MK (Fe XXI) plasma emissions (Lemen et al. 2012). Previously the 195 Å channel ( $\sim 1.6$  MK Fe XII and  $\sim 20$  MK Fe XXIV) has been used to identify  $^3\text{He}$ -rich SEPs sources (Nitta et al. 2006; Wang et al. 2006), but we found the brightening on the west limb easier to distinguish from the bright surroundings in the 131 Å EUV images. One interesting feature seen in the EUV 193 Å images was the presence of the large scale loops across the whole AR 11243 while such topology was not obvious in AR 11244. This is consistent with the PFSS model showing no open field in AR 11243 (see 2011-Jul-7.9 panel in Figure 5).

Although it is not clear whether the early 2011 July 8 electron event was accompanied by  $^3\text{He}$  emission (due to the data gap and elevated intensity from the previous activity) we check the solar source for these electrons. The associated B3.0 (02:53 UT) X-ray flare is assigned to AR 11243 in the NOAA/SWPC list. However, with the *STEREO-A* EUV images we see a quite impressive eruption in AR 11244 at the time of the B3.0 flare and only minor brightening in AR 11243. AR 11244 was  $\sim 2^\circ$  behind the west solar limb, but the expulsion was also well visible in the EUV images on *SDO*. The configuration of the modeled coronal fields shown in panel 2011-Jul-7.9 in Figure 5 would be valid also for the early 2011 July 8 electron event suggesting a most probable connection to AR 11244. Furthermore, we note from Figure 3a that the onset of this electron event is slower compared to the preceding electron events, which may be caused by the longer path length for electron propagation as AR 11244 rotated further away. We conclude that multiple electron events in Figure 3a, seen within a span of less than one day have the same solar origin - AR 11244. In the earlier surveys, multiple electron events within one day often originated in the same active region and have been often accompanied by a  $>1$  MeV nucleon $^{-1}$   $^3\text{He}$ -rich increase, but separate  $^3\text{He}$  increases were rarely identified (Reames et al. 1985). *STEREO-A* EUVI showed ongoing activity in AR 11244 on July 8 with multiple, smaller compared to the B3.0 flare, brightenings particularly between 10:00 and 11:00 UT, and at 21:15 UT. No type III bursts were recorded by WAVES instruments on *WIND* or *STEREO-A* s/c (Bougeret et al. 1995, 2008) in association with these brightenings. Also no associated electron events were detected by the near Earth s/c as seen in Figure 3a. A notable feature of AR 11244 was multiple surge-like ejections lasting almost a whole day, clearly visible on the west limb in AIA 304 Å EUV images.

#### 3.2.3. *ACE* 2011 July 9 Event

The low-latitude coronal hole, the *ACE* connection area for the 2011 July 9  $^3\text{He}$ -rich event, contained a small recently emerged bipolar active region, AR 11246, located at  $327^\circ$  Carrington longitude. The region was associated with three sunspots on 2011 July 8 as recorded in the SWPC SRS. We searched for activity in that solar region with particular focus on the period which precedes the beginning of the event. The *SDO* EUV images show that AR 11246 started to emerge on 2011 July 7 at  $\sim 23:00$  UT at the western edge of the coronal hole. On 2011 July 8 the AR was continuously growing, showing

two strong brightenings (at 11:40 and 14:40 UT) before the eruption at 16:30 UT. As viewed also in EUV, the size of AR 11246 ( $\sim 5 \times 10^4$  km) was much smaller than the neighboring AR 11243 or 11244. Figure 7 shows the emergence of this region in the 193 Å images from *SDO*. The upper panel of the figure shows the coronal hole when AR 11246 started to emerge and the lower panel the AR at the time when it likely stopped expanding. Notice that coronal holes in EUV images appear as relatively dark regions. The longitudinal extension of the coronal hole in EUV, between  $\sim 20^\circ$  and  $\sim 35^\circ$  in the upper panel of Figure 7, agrees well with the open field region from the PFSS calculation (refer to panel 2011-Jul-7.9 in Figure 5).

Figure 8 (upper panels) shows AR 11246 around the time of the eruption on 2011 July 8. The figure is a sequence of three 5-minute difference images from *SDO/AIA* 193 Å. The middle panel shows collimated or jet-like emissions at the northern footpoint of the bigger flaring loop (there is likely also a small inner loop) which is located close to the coronal hole boundary (refer to Figure 7). The  $\lambda$ -shaped structure appears to be consistent with the general scenario of jets created by reconnection between open and closed field lines (Shibata et al. 1992; Wang et al. 1998). The lower panel in Figure 8 shows all three ARs 11246, 11243 and 11244 in the 5-minute difference image from *STEREO-A* 195 Å EUVI on 2011 July 8 16:25 UT. One can see the most prominent brightening in AR 11246 located at E55°. Note that due to projection effects, bright features in AR 11246 appear smaller than in AR 11244 which is located near the central meridian (W05°). AR 11246 produced several other eruptions on 2011 July 9-10 after the SEP event start time. On July 11 the AR had rotated close to the west solar limb and was barely visible with *SDO*. But at that time *STEREO-A* EUVI was able to see AR 11246 near the central meridian with continuing activity. The AR decayed in the middle of 2011 July 12, but it still produced sporadic jets on 2011 July 13-14 before the region re-emerged with an even smaller size at the end of July 14.

### 3.2.4. *STEREO-A* 2011 July 16 Event

It has been shown that *STEREO-A* was connected to the same low-latitude coronal hole during the 2011 July 16  $^3\text{He}$ -rich period. In contrast to the previous case there were two new bright solar regions in the vicinity of the coronal hole, one relatively small region beneath the coronal hole southern boundary (hereafter A1) and a larger one (hereafter A2)  $\sim 10^\circ$  west of AR 11246. The region A1 started to emerge on 2011 July 11 and A2 on 2011 July 10. When it started to emerge the larger region A2 was at  $\sim \text{N}08^\circ\text{W}80^\circ$  as viewed from the Earth and reached its full size behind the solar west limb. Therefore the region does not clearly show up in the photospheric maps and the PFSS extrapolations probably could not properly determine the open field region. The limitations of the PFSS model for unobserved areas especially above rapidly evolving active regions have been discussed by Nitta & DeRosa (2008).

Figure 9 shows the activity just before the start of the 2011 July 16  $^3\text{He}$ -rich period, showing the larger area west of the coronal hole. The upper panel displays

the *STEREO-A* 195 Å EUV image on 2011 July 15 at 22:25 UT. The lower panel is the difference between the two EUV images taken at 22:25 and 22:20 UT. In the difference image we can see jet-like emission at the western edge of the coronal hole and no significant brightening in other regions. The site of this jet coincides with Carrington longitude of AR 11246. The coronal hole seen in *STEREO-A* EUVI reveals the presence of the open field region, as inferred from the model field. The region A2 showed one material eruption and one brightening in the first half of July 15. Careful inspection of this region in the EUV 195 Å images reveals a closed magnetic field configuration for most of the time presumably preventing any energetic particles from escaping. The region A1 showed no significant brightening in EUV.

In addition to the jet in AR 11246 seen near the end of the day, the region showed three distinct brightenings earlier on July 15 at 12:40, 14:15 and 18:45 UT. Figure 10 shows these brightenings in a wider area of the western hemisphere to demonstrate that no other regions were simultaneously active. Bright patches on the west limb were associated with AR 11244. *STEREO-B* saw AR 11244 at  $\sim \text{E}80^\circ$ , and obtained higher cadence (2.5-min) EUV 195 Å images but revealed no exceptional activity. From the figure we can see, that brightenings in AR 11246 do not have a collimated ejection or jet-like structure. It has been previously reported that some sources of  $^3\text{He}$  show only amorphous brightening (Wang et al. 2006). Those authors pointed out that a jet could have been missed because of the low time cadence (12-minute) of the EUV observations available. In our case missed jets would have a duration less than 5 minutes. It is important to note that during the jets and brightenings in AR 11246 on July 15, *STEREO-A* was magnetically connected via negative field to nearby AR 11243.

### 3.3. Radio Observations Associated with 2011 July 9 and July 16 Events

Figure 11 (upper panel) shows the *STEREO-A*/WAVES radio spectrogram for the second half of 2011 July 15 with several type III bursts. It is interesting that all three brightenings in AR 11246 on July 15, marked by arrows in Figure 11, coincide with prominent type III emissions. This indicates that electrons are accelerated in this region and escape into the interplanetary medium along the open field lines. These three bursts are characterized by similar frequency-time profiles and extend to the local plasma frequency at 1 AU ( $\leq 50$  kHz e.g., Cane 2003). Note that the jet at 22:25 UT (not marked in the radio spectrogram) was associated with a narrow type III burst which does not extend down to the low frequencies as in the previous three cases implying that the causative electrons probably did not reach  $\sim 1$  AU. Temporal association of type III radio bursts with EUV jets in solar impulsive electron events has been reported in recent studies (Klassen et al. 2011; Li et al. 2011). Further exploration of *STEREO-A* radio data shows that there were no significant type III bursts found on 2011 July 16 before the event start time.

We have also examined the *WIND*/WAVES radio spectrogram of 2011 July 8. Except for a type III burst associated with the electron event at the beginning of the day there were two other significant type III emissions on

July 8 with start times at 11:37 and 16:25 UT as shown in the lower panel in Figure 11. The first one is associated with the eastern hemisphere AR 11247 and C2 class flare in the NOAA/SWPC flare list, and the second one does not have any source association in the list. However, at the time of the second type III burst (16:25 UT) the *SDO* EUV images showed a jet-like eruption in AR 11246 displayed in Figure 8. Such temporal coincidence implies their common origin and indicates energetic electrons escaping from AR 11246 into interplanetary space. We remark that the L1 s/c were in a negative magnetic polarity sector at the time of jet-like eruption and thus not connected to AR 11246 at the periphery of the coronal hole. We note another brightening mentioned in Section 3.2.3 in *SDO*/AIA EUV observations in AR 11246 on July 8 just close to the time of the type III burst at 11:37 UT. This may imply a false association of this type III burst with AR 11247 in the SWPC list.

#### 4. SUMMARY AND DISCUSSION

We have examined  $^3\text{He}$ -rich periods of SEPs observed consecutively by the *STEREO-B*, *ACE*, and *STEREO-A* spacecraft when they were widely separated in longitude. The period observed by *ACE* consists of two distinct  $^3\text{He}$ -rich events. The period observed by *STEREO-B* on 2011 July 1 and later by *ACE* on 2011 July 7 was associated with a sizeable active region, AR 11244. The AR produced energetic electron events with associated type III bursts, soft X-ray flares and a  $\text{H}\alpha$ -flare. The period is characterized by a moderate  $^3\text{He}$ -enrichment ( $^3\text{He}/^4\text{He} < 1$ ). The period observed by *ACE* on 2011 July 9 and later by *STEREO-A* on 2011 July 16 was presumably associated with the small, compact AR 11246 located at the border of the coronal hole and showed very high  $^3\text{He}$ -enrichment and fluence, the highest so far detected on *STEREO*. The source region produced EUV jets correlated with type III bursts and exhibited highly dynamic behavior. For example, when the active region temporarily disappeared the site continued with jet-like emissions. The characteristics of the events in this study are consistent with earlier suggestions that small flares have probably more favorable conditions for the  $^3\text{He}$  enrichments of SEPs than large flares (Reames et al. 1988), and that different size or morphology of the source active region with diverse flaring could produce a  $^3\text{He}$ -rich event (Kahler et al. 1987).

In spite of a dispersionless onset and absence of energetic electrons in the July 9 and 16 events the high cadence EUV images combined with the radio observations allowed us to determine the likely source brightening for the  $^3\text{He}$  emission. The approximate travel time of solar  $^3\text{He}$  ions with an energy 0.23–0.32 MeV nucleon $^{-1}$  is about 7 hours to *ACE* along a nominal spiral with length of 1.2 AU. If the  $^3\text{He}$  was released during the eruption in AR 11246 at 16:30 UT on 2011 July 8 the ions with that energy should have been detected at the beginning of July 9, which is approximately consistent with the start of the event in the low energy time-intensity profile in Figure 3b. Since the s/c was not connected to the coronal hole (and to the source AR) around the eruption time it missed the electrons and the first-arriving, higher-energy ions. This explains the lack of velocity dispersion in the ions received after the s/c enters the field lines connected to the coronal hole. If the release of the energetic ions

for the 2011 July 16 period was associated for example with the jet and type III radio burst at 22:25 UT on July 15 then the lowest energy ions (0.18 MeV) shown in Figure 4c should arrive at *STEREO-A* around 06:30 UT on July 16 (i.e., three hours before the dispersionless event onset). If the ions were released during the brightening at 18:45 UT, which was associated with the prominent type III burst, the highest energy ions (1.49 MeV) should have only a  $\sim 3$  hr delay after the flare. This leads to the question of where these high energy solar ions, with enormous  $^3\text{He}$  enrichment, were residing in the heliosphere for about half of the day prior to the observed onset.

The timing of the ion intensities in the 2011 July 16 period indicates that energetic  $^3\text{He}$  is closely associated with the CIR which is further supported by the pre- and post-event abundances. Such association may arise when a source active region is located at the periphery of the coronal hole with open field lines bending to the ecliptic. The high-speed solar wind emanating from the hole may create a corotating compression region in the heliosphere near  $\sim 1$  AU. Thus the energetic  $^3\text{He}$  injected from the solar source near the hole is guided by the open field to the CIR. The propagation of SEPs in the compressed field in CIRs has been modeled by Kocharov et al. (2003). The authors employed the Giacalone et al. (2002) model of CIR acceleration on the solar wind speed gradients at 1 AU. Their simulations show that the magnetic enhancement associated with the CIR presents a kind of magnetic mirror away from the Sun where solar particles may be temporally trapped and re-accelerated. Indeed, our observations show a significant sunward component during the 2011 July 16  $^3\text{He}$ -rich period indicating a reflecting boundary beyond the observer. Kocharov et al. (2008) have reported on multi-day  $^3\text{He}$ -rich periods that essentially all have dispersionless onset and were associated with compression in the solar wind but such convincing associations as in the July 16 period have not been presented. Those authors suggest that confinement of particles in CIRs is a significant factor of extended  $^3\text{He}$ -rich periods of SEPs.

It is not clear if the weaker CIR seen during the 2011 July 9  $^3\text{He}$ -rich period had a marked influence on the SEPs. The event commenced with a change of the magnetic connection and not with the start of the solar wind speed rise or at the CIR stream interface although the later was not fully developed. Presumably at larger radial distances where the corotating compression regions are found to be stronger, a closer association might exist. Kocharov et al. (2003) concluded that the effects of the compression may be important if the observed solar wind speed increase near Earth is more than 100 km s $^{-1}$  within a few hours. In the 2011 July 9 CIR, such a speed change is observed during a quite long  $\sim 12$  hr period. Notice that no significant concurrent CIR event was observed in association with the 2011 July 9 and July 16 compression corotating regions. That means at least for the strong July 16 compression that the bulk solar wind was not accelerated in the CIR. It is consistent with recent suggestions that CIR ions are accelerated out of the suprathermal ion pool (Mason et al. 2012). In the case of the July 16 CIR the suprathermal population was probably dominated by the  $^3\text{He}$ -rich SEPs which might undergo acceleration in the strong compression region.

These small SEP events are often difficult to conclu-



sively identify with source activity in active periods when there may be multiple candidates. In the July 9 event the s/c footpoint lies in a reasonable distance from both ARs 11246 and 11244. Note that the distance to AR 11244 was still within  $3\sigma$  ( $\sim 48^\circ$ ) of the flare longitudes distribution associated with  $^3\text{He}$ -rich SEP events derived by Reames (1999). There are a few reasons to choose AR 11246 over AR 11244. The type III emissions at 11:37 and 16:25 UT preceding the July 9 event were probably associated with AR 11246 because of their temporal coincidence with the EUV brightenings in this AR; the brightenings, fainter at these times in AR 11244 were not new and likely continued from the previous activity. If the type III burst at 16:25 UT was associated with AR 11244 then why do we not detect escaping electrons, while being in a negative IMF sector and presumably connected to AR 11244? Another reason in favor of AR 11246 is the reversal of the IMF to the polarity at AR 11246 at the start of the July 9 event. Although AR 11244 continued with some activity on July 15-16, the type III bursts at 12:40, 14:15 and 18:45 UT on July 15 appear to be correlated with EUV brightenings in AR 11246. Note that some ambiguity may still remain in locating these type III bursts because we use lower (5 minute) cadence EUVI data. *WIND*/*WAVES* observed weak and only low-frequency counterparts of these bursts. *STEREO-B*/*WAVES* did not record any type III emission on July 15 in the same time period as *STEREO-A*. This implies that the source was well hidden from the *STEREO-B* view, which was not case of AR 11244. In addition, the AR 11244 location is less likely to be the source for the  $^3\text{He}$ -rich event on *STEREO-A*. We have shown that the *STEREO-A* footpoint was co-located with the coronal hole (containing AR 11246), while AR 11244 was quite far,  $60^\circ$  west of the footpoint.

In conclusion, with the advantage of widely separated spacecraft carrying advanced imaging, radio and particle instrumentation, supported by the modeling of the coronal field, we have identified solar ARs which exhib-

ited repeated energetic electron and  $^3\text{He}$  emissions for a relatively long interval of time, up to about a quarter of a solar rotation. This is significantly longer than single s/c observations which previously reported  $^3\text{He}$  injections from the same AR over a period of one day. Thus this study suggests that the conditions for the  $^3\text{He}$  acceleration in a single solar region may persist for a long time. Furthermore the observations in this paper show that a recurrent  $^3\text{He}$ -rich period can be preserved in the solar wind by confining SEPs in the CIR. The observations of a long-lived recurrent period presented in this study may provide new insights on the acceleration of  $^3\text{He}$  ions in the solar flares and their transport in the heliosphere. In particular, extended  $^3\text{He}$ -rich periods recently discovered with single s/c observations may be naturally explained by multiple injections from the same AR which may presumably last over days.

This work was supported by the Bundesministerium für Wirtschaft through the Deutsches Zentrum für Luft- und Raumfahrt (DLR) under grant 50 OC 0904. The work at JHU/APL was supported by NASA under contract SA4889-26309 from the University of California Berkeley and by NASA grants 44A-1089749 and NNX13AR20G. R. Gómez-Herrero acknowledges the financial support from the Spanish Ministerio de Ciencia e Innovación under project AYA2011-29727-C02-01. The *STEREO*/SEPT project is supported by DLR grant 50 OC 1302. The authors thank M. E. Wiedenbeck for providing the *STEREO*/LET helium mass spectrogram plots. We acknowledge the National Space Science Data Center (NSSDC), Space Physics Data Facility (SPDF) and PI K. W. Ogilvie at GSFC and A. J. Lazarus at MIT for use of the *WIND*/SWE data. We thank the *ACE* SWEPAM/EPAM/MAG and the *STEREO* PLASTIC instrument teams for the use of the solar wind plasma data.

## REFERENCES

- Acuña, M. H., Curtis, D., Scheifele, J. L., et al. 2008, *SSRv*, 136, 203
- Barnes, C. W., & Simpson, J. A. 1976, *ApJ*, 210, L91
- Bougeret, J. L., Goetz, K., Kaiser, M. L., et al. 2008, *SSRv*, 136, 487
- Bougeret, J.-L., Kaiser, M. L., Kellogg, P. J., et al. 1995, *SSRv*, 71, 231
- Bučík, R., Innes, D. E., Mall, U., Korth, A., & Mason, G. M. 2013a, in *Proc. 33rd ICRC (Rio de Janeiro)*, paper SH-EX 0552 (arXiv:1307.6342)
- Bučík, R., Mall, U., Korth, A., & Mason, G. M. 2012, *SoPh*, 281, 411
- Bučík, R., Mall, U., Korth, A., Mason, G. M., & Gómez-Herrero, R. 2013b, in *AIP Conf. Proc.*, 1539, 139
- Burlaga, L. F. 1995, *Interplanetary magnetohydrodynamics, International Series on Astronomy and Astrophysics* (New York: Oxford Univ. Press)
- Cane, H. V. 2003, *ApJ*, 598, 1403
- Chottoo, K., Schwadron, N. A., Mason, G. M., et al. 2000, *JGRA*, 105, 23107
- Crooker, N. U., Gosling, J. T., Bothmer, V., et al. 1999, *SSRv*, 89, 179
- Galvin, A. B., Kistler, L. M., Popecki, M. A., et al. 2008, *SSRv*, 136, 437
- Giacalone, J., Jokipi, J. R., & Kóta, J. 2002, *ApJ*, 573, 845
- Gold, R. E., Krimigis, S. M., Hawkins, S. E., et al. 1998, *SSRv*, 86, 541
- Gosling, J. T., Asbridge, J. R., Bame, S. J., & Feldman, W. C. 1978, *JGRA*, 83, 1401
- Gosling, J. T., & McComas, D. J. 1987, *GeoRL*, 14, 355
- Gómez-Herrero, R., Malandraki, O., Dresing, N., et al. 2011, *JASTP*, 73, 551
- Howard, R. A., Moses, J. D., Vourlidas, A., et al. 2008, *SSRv*, 136, 67
- Jian, L., Russell, C. T., Luhmann, J. G., Skoug, R. M. 2006, *SoPh*, 239, 337
- Kahler, S. W., Lin, R. P., Reames, D. V., Stone, R. G., & Liggett, M. 1987, *SoPh*, 107, 385
- Klassen, A., Gómez-Herrero, R., & Heber, B. 2011, *SoPh*, 273, 413
- Klein, L., & Burlaga, L. F. 1980, *JGRA*, 85, 2269
- Klein, K.-L., Krucker, S., Lointier, G., & Kerdraon, A. 2008, *A&A*, 486, 589
- Kocharov, L. G., & Kocharov, G. E. 1984, *SSRv*, 38, 89
- Kocharov, L., Kovaltsov, G. A., Torsti, J., Anttila, A., Sahla, T. 2003, *JGRA*, 108, 1404
- Kocharov, L., Laivola, J., Mason, G. M., Didkovsky, L., & Judge, D. L. 2008, *ApJS*, 176, 497
- Lemen, J. R., Title, A. M., Akin, D. J., et al. 2012, *SoPh*, 275, 17
- Li, C., Matthews, S. A., van Driel-Gesztelyi, L., Sun, J., & Owen, C. J. 2011, *ApJ*, 735, 43
- Lin, R. P. 1974, *SSRv*, 16, 189
- Lin, R. P., Anderson, K. A., Ashford, S., et al. 1995, *SSRv*, 71, 125
- Lin, R. P., Curtis, D. W., Larson, D. E., et al. 2008, *SSRv*, 136, 241
- Mason, G. M. 2007, *SSRv*, 130, 231
- Mason, G. M., Desai, M. I., & Li, G. 2012, *ApJ*, 748, L31
- Mason, G. M., Desai, M. I., Mall, U., et al. 2009, *SoPh*, 256, 393
- Mason, G. M., Dwyer, J. R., & Mazur, J. E. 2000, *ApJ*, 545, L157

- Mason, G. M., Gold, R. E., Krimigis, S. M., et al. 1998, SSRv, 86, 409
- Mason, G. M., Korth, A., Walpole, P. H., et al. 2008, SSRv, 136, 257
- Mason, G. M., Mazur, J. E., & Dwyer, J. R. 1999, ApJ, 525, L133
- Mason, G. M., Mazur, J. E., Dwyer, J. R., Reames, D. V., & von Rosenvinge, T. T. 1997, ApJ, 486, L149
- Mason, G. M., Mazur, J. E., Dwyer, J. R., et al. 2004, ApJ, 606, 555
- McComas, D. J., Bame, S. J., Barker, P., et al. 1998, SSRv, 86, 563
- Mewaldt, R. A., Cohen, C. M. S., Cook, W. R., et al. 2008, SSRv, 136, 28
- Müller-Mellin, R., Böttcher, S., Falenski, J., et al. 2008, SSRv, 136, 363
- Nitta, N. V. & DeRosa, M. L. 2008, ApJ, 673, L207
- Nitta, N. V., Mason, G. M., Wiedenbeck, M. E., et al. 2008, ApJ, 675, L125
- Nitta, N. V., Reames, D. V., DeRosa M. L., et al. 2006, ApJ, 650, 438
- Nolte, J. T., & Roelof, E. C. 1973, SoPh, 33, 241
- Ogilvie, K. W., Chornay, D. J., Fritzenreiter, R. J., et al. 1995, SSRv, 71, 55
- Pick, M., Mason, G. M., Wang, Y.-M., Tan, C., & Wang, L. 2006, ApJ, 648, 1247
- Reames, D. V. 1990, ApJS, 73, 235
- Reames, D. V. 1999, SSRv, 90, 413
- Reames, D. V., Denis, B. R., Stone, R. G., & Lin, R. P. 1988, ApJ, 327, 998
- Reames, D. V., von Rosenvinge, T. T., & Lin, R. P. 1985, ApJ, 292, 716
- Reames, D. V., & Stone, R. G. 1986, ApJ, 308, 902
- Richardson, I. G., Barbier, L. M., Reames, D. V., & von Rosenvinge, T. T. 1993, JGRA, 98, 13
- Richardson, I. G., & Cane, H. V. 1995, JGRA, 100, 23397
- Richardson, I. G., & Zwickl, R. D. 1984, P&SS, 32, 1179
- Sauvaud, J.-A., Larson, D., Aoustin, C., et al. 2008, SSRv, 136, 227
- Schatten, K. H., Wilcox, J. M., & Ness, N. F. 1969, SoPh, 6, 442
- Schrijver, C. J., & DeRosa, M. L. 2003, SoPh, 212, 165
- Shibata, K., Ishido, Y., Acton, L. W., et al. 1992, PASJ, 44, L173
- Smith, C. W., L'Heureux, J., Ness, N. F., et al. 1998, SSRv, 86, 613
- Stone, E. C., Cohen, C. M. S., Cook, W. R., et al. 1998, SSRv, 86, 357
- Tsurutani, B. T., Zhang, L. D., Mason, G. M., et al., 2002, AnGeo, 20, 427
- Wang, L., Lin, R. P., Salem, C. et al., 2012, ApJ, 753, L23
- Wang, Y.-M., Pick, M., & Mason, G. M. 2006, ApJ, 639, 495
- Wang, Y.-M., Sheeley, N. R., Jr., Socker, D. G., et al. 1998, ApJ, 508, 899
- Zwickl, R. D., Roelof, E. C., Gold, R. E., & Krimigis, S. M. 1978, ApJ, 225, 281

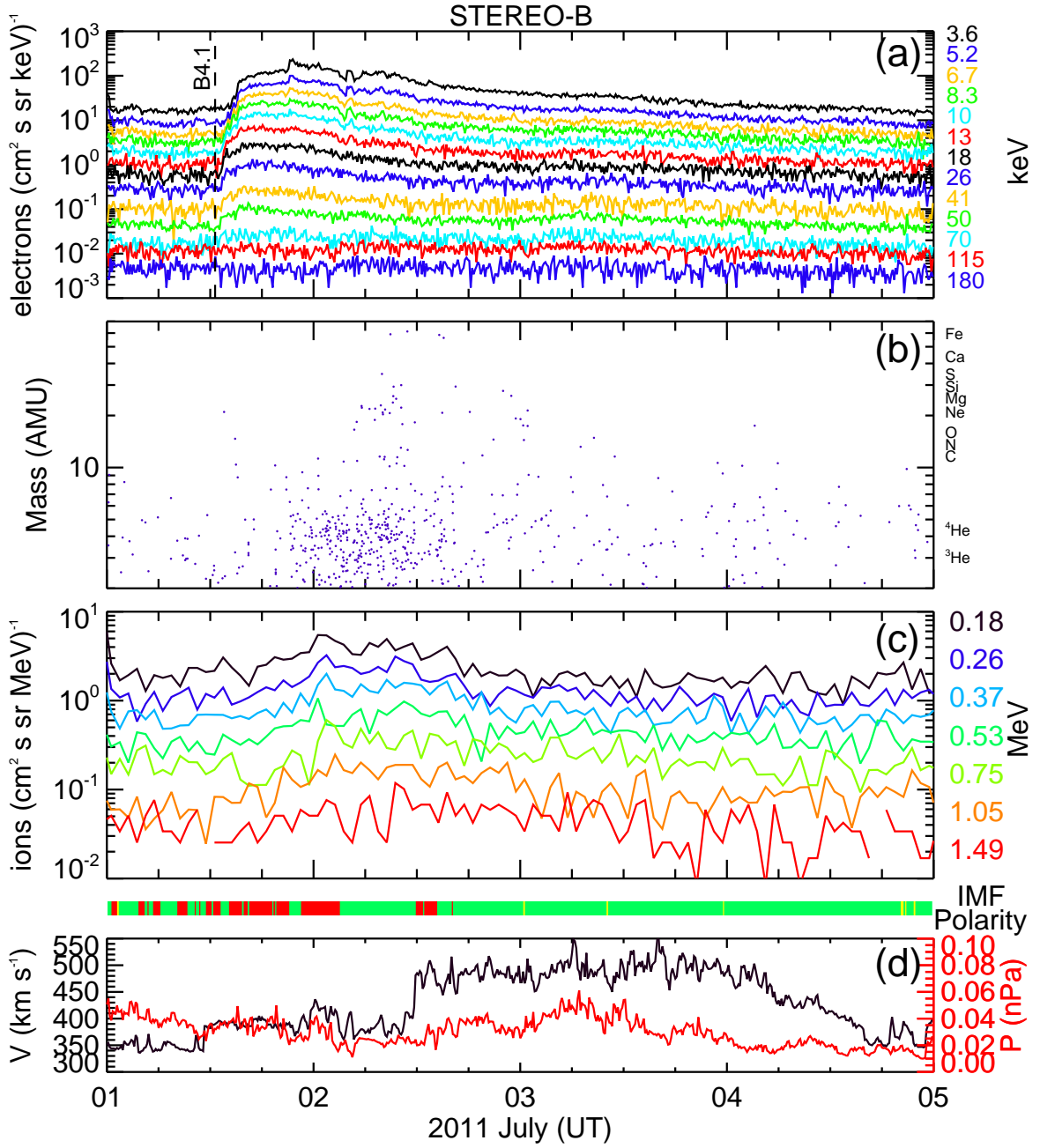


FIG. 1.— (a) 10-min *STEREO-B*/STE D3 (3.6-41 keV) electron intensities from one of the four downstream (looking in anti-sun direction) STE detectors and 10-min *STEREO-B*/SEPT (50-180 keV) electron intensities from the sunward pointing sensor. The dashed vertical line indicates the start time of the GOES B4.1 X-ray flare. (b) *STEREO-B*/SIT mass spectrogram of individual ions in the energy ranges 0.25-0.90 MeV nucleon $^{-1}$  (mass <8 amu) and 0.08-0.15 MeV nucleon $^{-1}$  (mass >8 amu). (c) 1-hr *STEREO-B*/SEPT (0.18-1.49 MeV) ion intensities from the sunward pointing sensor. (d) 10-min solar wind speed  $V$  (black curve) and 10-min total pressure  $P$  (red curve). IMF polarity color bar indicates by red (green) the times when the observed magnetic field vector was oriented toward (away from) the Sun. The yellow indicates the times with ambiguous polarity.

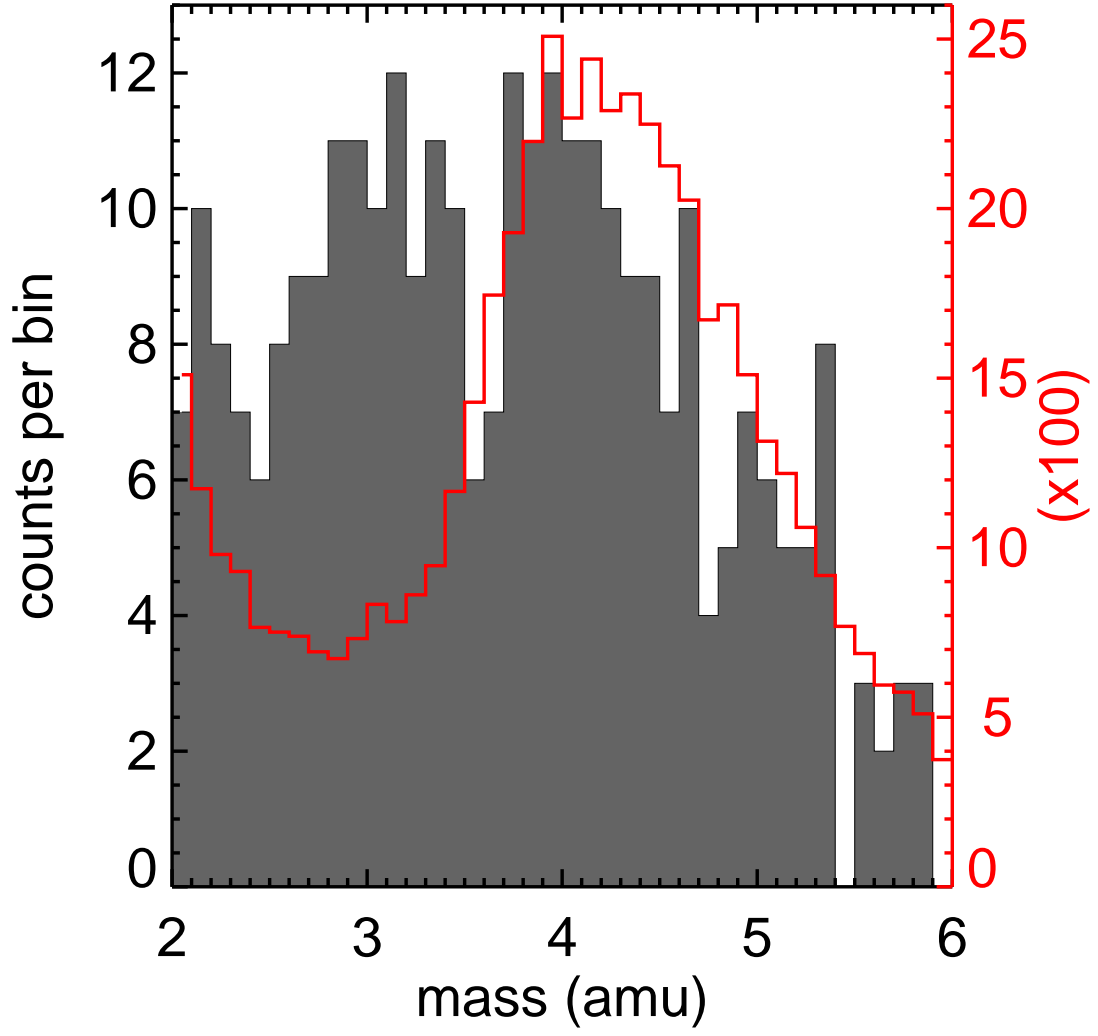


FIG. 2.— *STEREO-B/SIT* He mass histograms in the energy range  $0.25\text{--}0.9\text{ MeV nucleon}^{-1}$  for 2011 July 1  $^3\text{He}$ -rich period (gray shaded) and for an intense CIR event on 2010 August 19-21 (red curve).

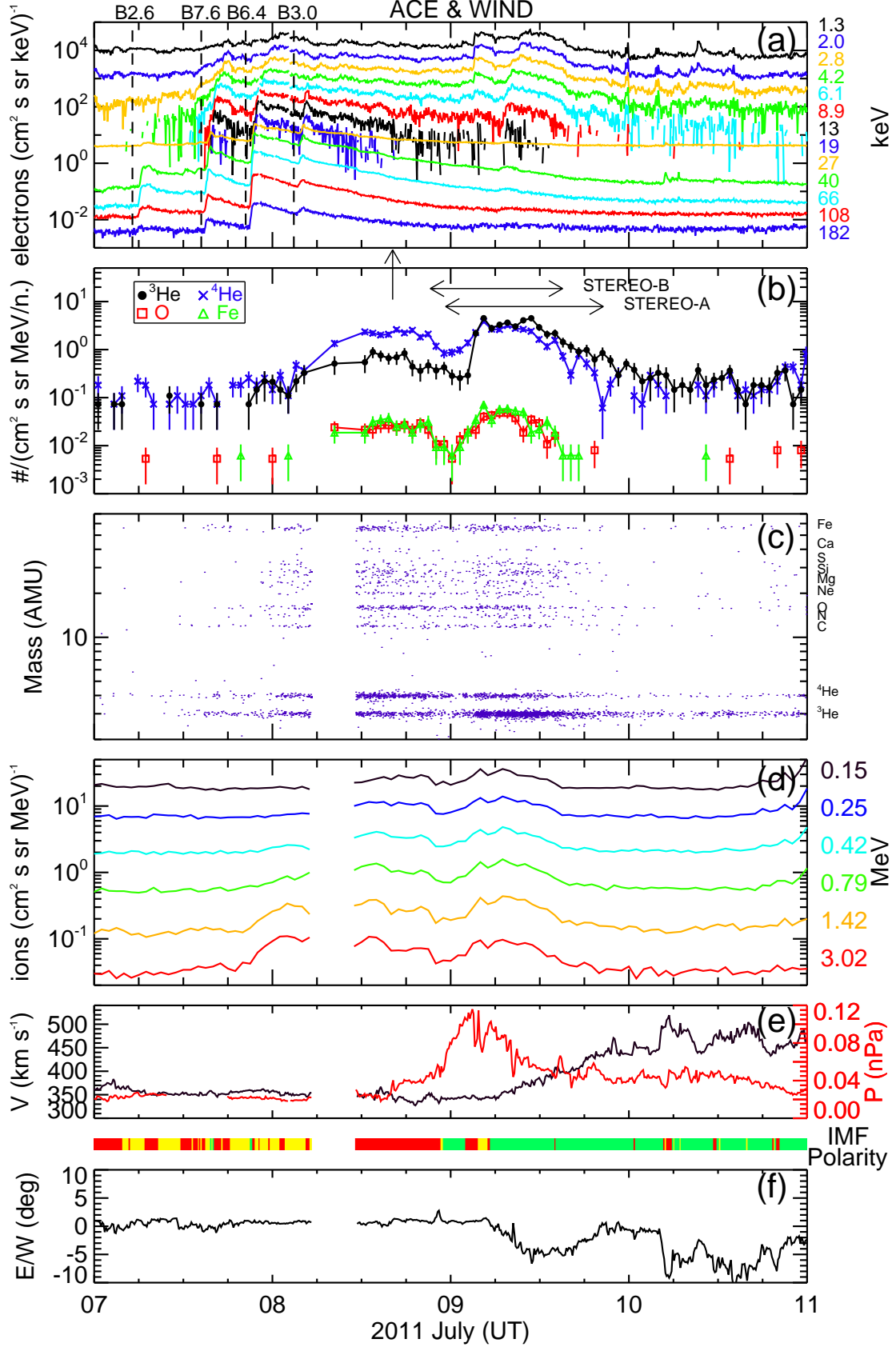


FIG. 3.— (a) 5-min *WIND*/3DP electron intensities from EESA-H (1.3–19 keV) and SST (27–182 keV) telescopes. Dashed vertical lines indicate start times of the related *GOES* soft X-ray flares. The arrow indicates an EUV jet in AR 11246. (b) 1-hr *ACE*/ULEIS 0.23–0.32 MeV nucleon $^{-1}$   $^4\text{He}$ ,  $^3\text{He}$ , O, Fe intensity. (c) 0.4–10 MeV nucleon $^{-1}$  *ACE*/ULEIS mass spectrogram. (d) 1-hr *ACE*/EPAM (0.15–3.02 MeV) ion intensities from LEMS120 detector. (e) 10-min solar wind speed  $V$  (black curve) and 10-min total pressure  $P$  (red curve). (f) 10-min azimuthal solar wind flow angle in Radial-Tangential-Normal (RTN) coordinates. Positive angles correspond to flow in the direction of solar rotation (westward). IMF polarity color bar has the same meaning as in Figure 1.

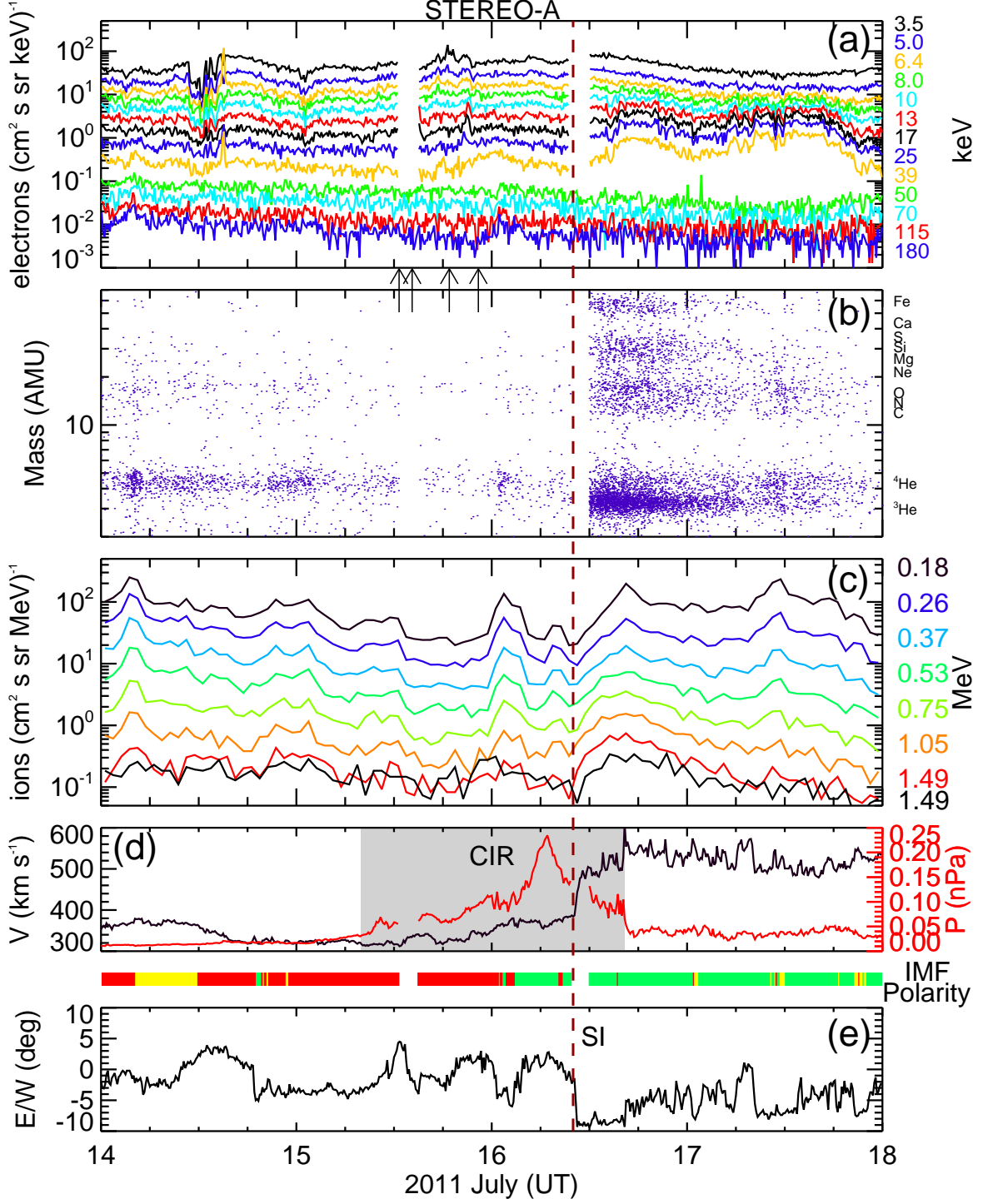


FIG. 4.— (a) 10-min electron intensities from *STEREO-A*/STE D3 (3.5-39 keV) anti-sunward and *STEREO-A*/SEPT (50-180 keV) sunward pointing sensors. Arrows indicate EUV brightenings and a jet in AR 11246. (b) *STEREO-A*/SIT mass spectrogram as in Figure 1b. (c) 1-hr *STEREO-A*/SEPT (0.18-1.49 MeV) ion intensities from the sunward pointing sensor and from the anti-sunward sensor for one energy channel centered at 1.49 MeV (lower black curve). (d) 10-min solar wind speed  $V$  (black curve) and 10-min total pressure  $P$  (red curve). Grey shaded region marks the time interval of the CIR. Dashed vertical line indicates solar wind stream interface (SI). (e) 10-min azimuthal solar wind flow angle in RTN coordinates. IMF polarity color bar has the same meaning as in Figure 1.

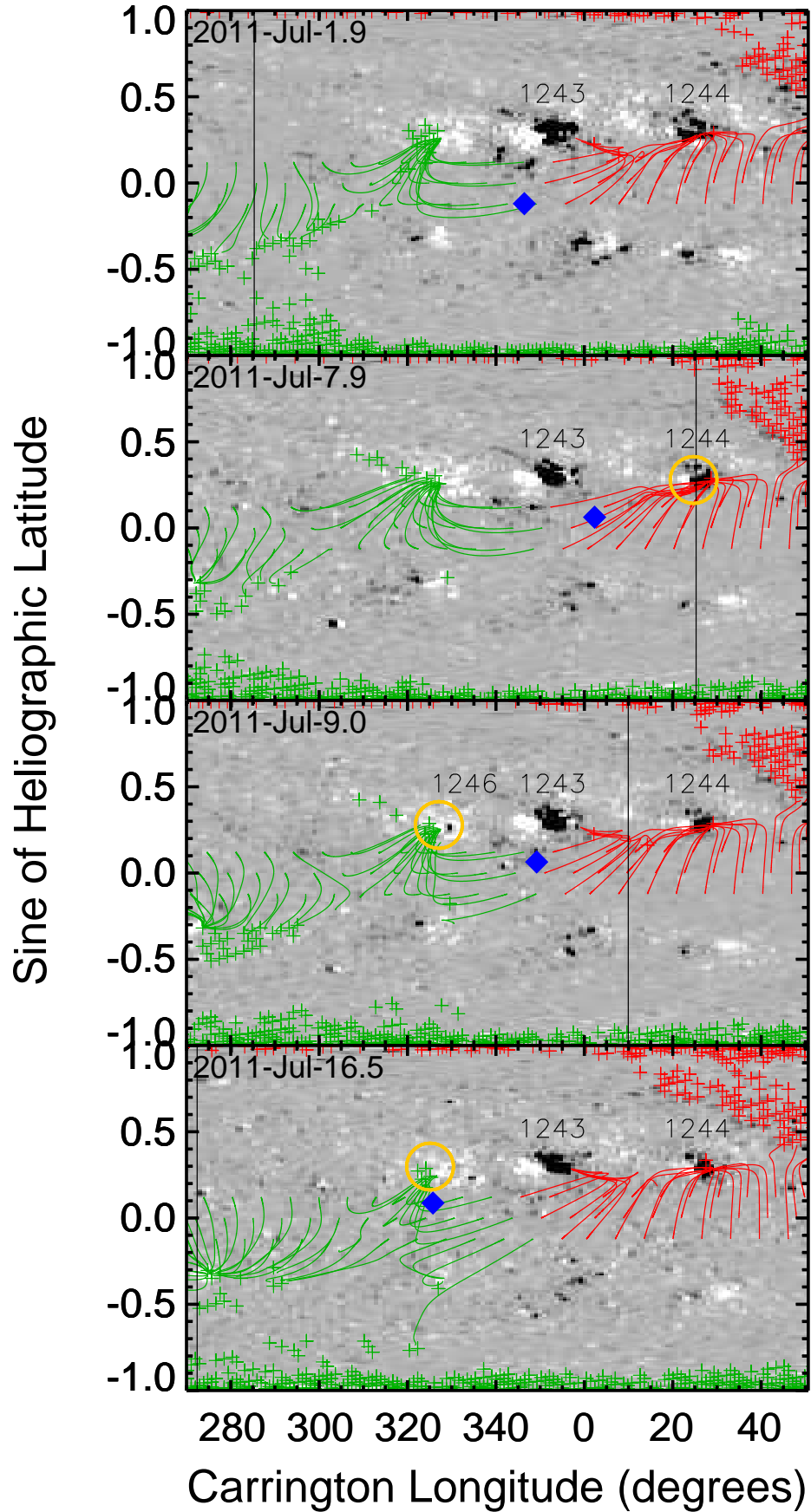


FIG. 5.— Photospheric magnetic field scaled to  $\pm 30 \text{ Mx cm}^{-2}$  (gray scale) with PFSS model coronal field lines (red and green) at the start time (as date and fraction of day) of the  $^3\text{He}$ -rich events. Shown are field lines which intersect source surface at latitudes  $0^\circ$  and  $\pm 7^\circ$ . Red/green indicates negative/positive open field. Blue diamonds mark *STEREO-B* (top panel), *L1* (two middle panels) and *STEREO-A* (bottom panel) footpoints on the source surface. Black vertical lines mark east (top panel) and west (three lower panels) solar limb from the Earth view point. Yellow circles (three lower panels) indicate the s/c connection location on the Sun. NOAA ARs 11243, 11244 and 11246 are indicated. Note that time runs from right to left in the maps.



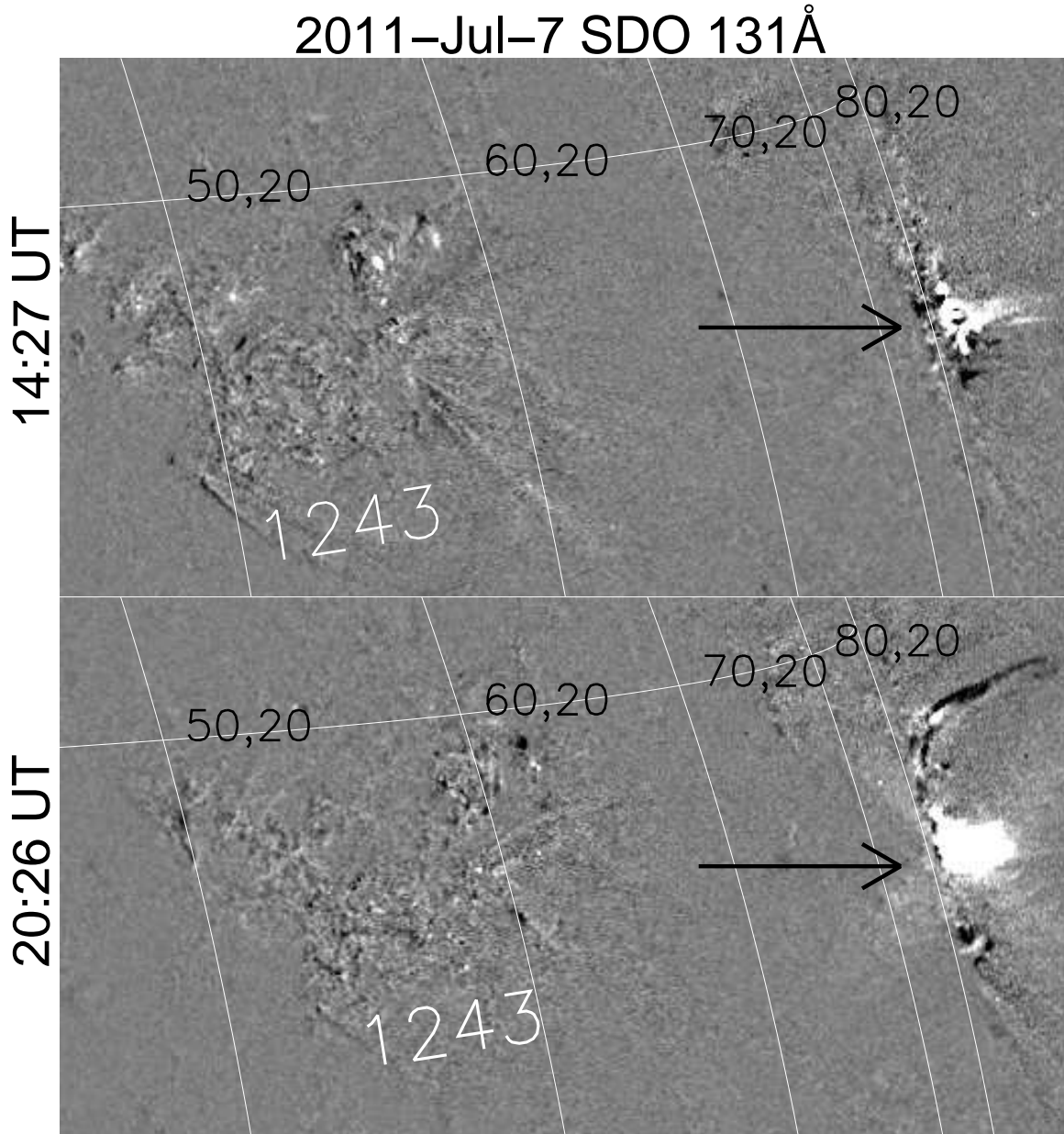


FIG. 6.— EUV 131 Å *SDO/AIA* four-minute difference images near the times of B7.6 (upper panel) and B6.4 (lower panel) X-ray flares on 2011 July 7; white (black) indicates increasing (decreasing) emission over the difference time interval. Black arrows point to the brightenings in AR 11244. AR 11243 and the heliographic longitude - latitude grid are labeled.



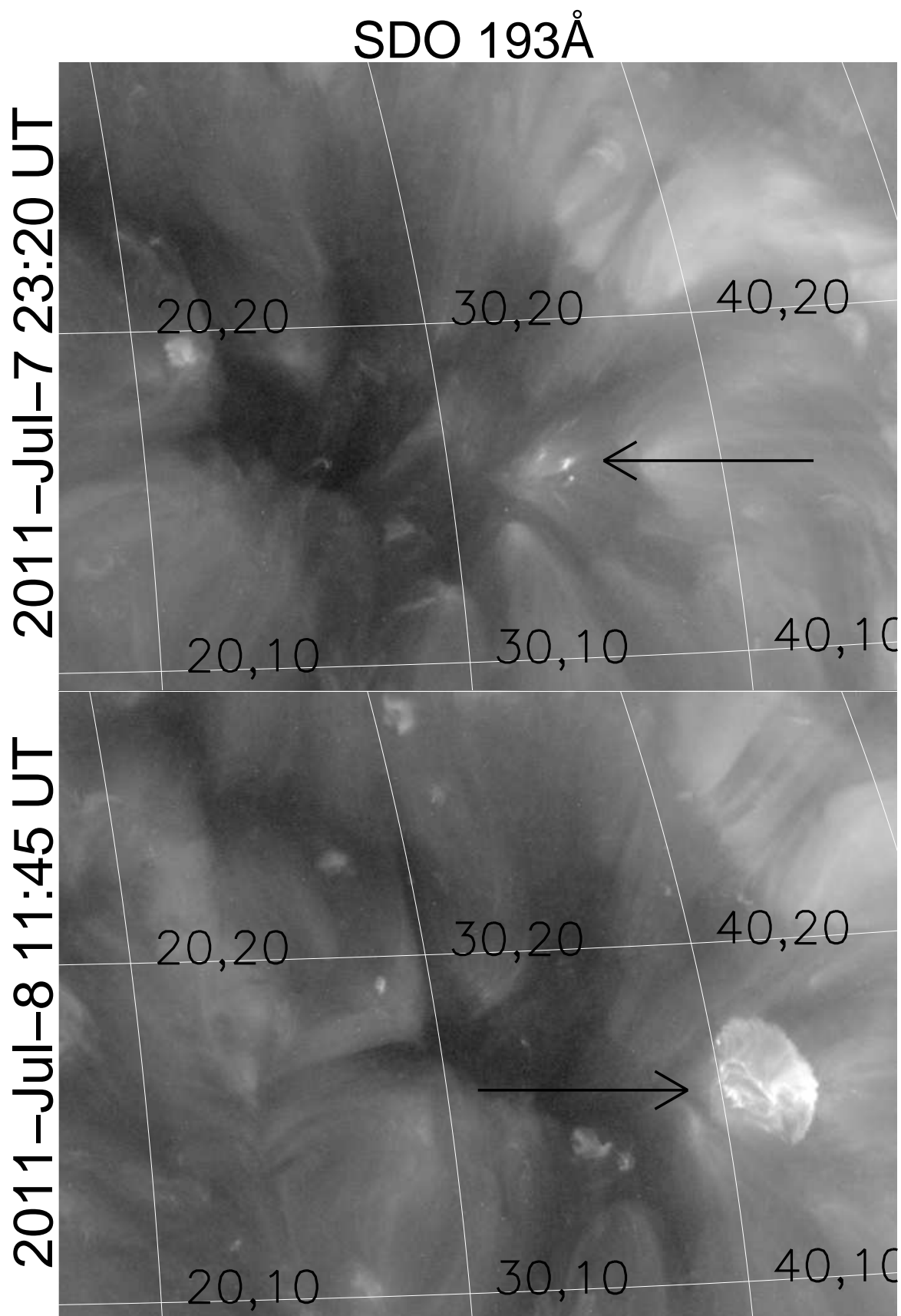


FIG. 7.— EUV 193 Å *SDO/AIA* images of the coronal hole on 2011 July 7 at 23:20 UT (upper panel) and on 2011 July 8 at 11:45 UT (lower panel). Black arrow marks an emergence of AR 11246. Heliographic longitude - latitude grid with labels in degrees is displayed.

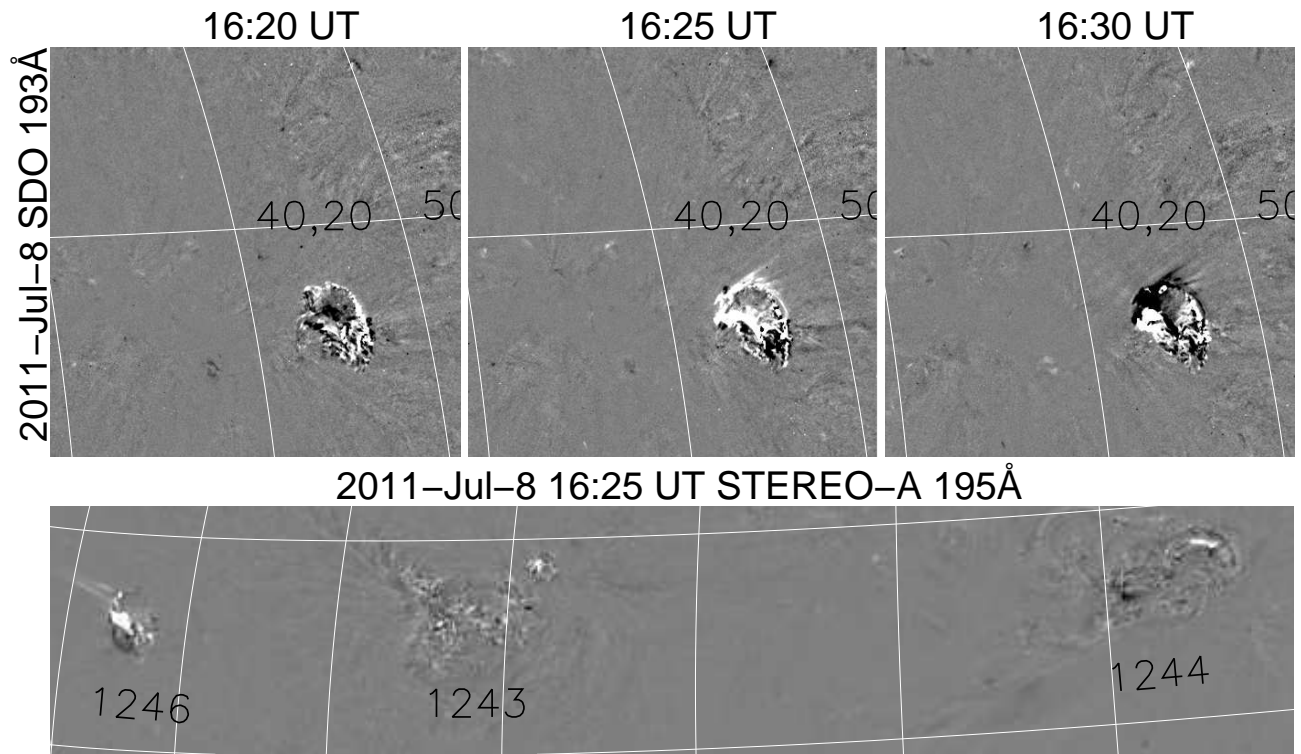


FIG. 8.— 5-minute difference EUV 193 Å *SDO/AIA* (upper panels) and 195 Å *STEREO-A/SECCHI* (lower panel) images on 2011 July 8 near the eruption time of AR 11246.

2011-Jul-15 22:25 UT STEREO-A 195Å

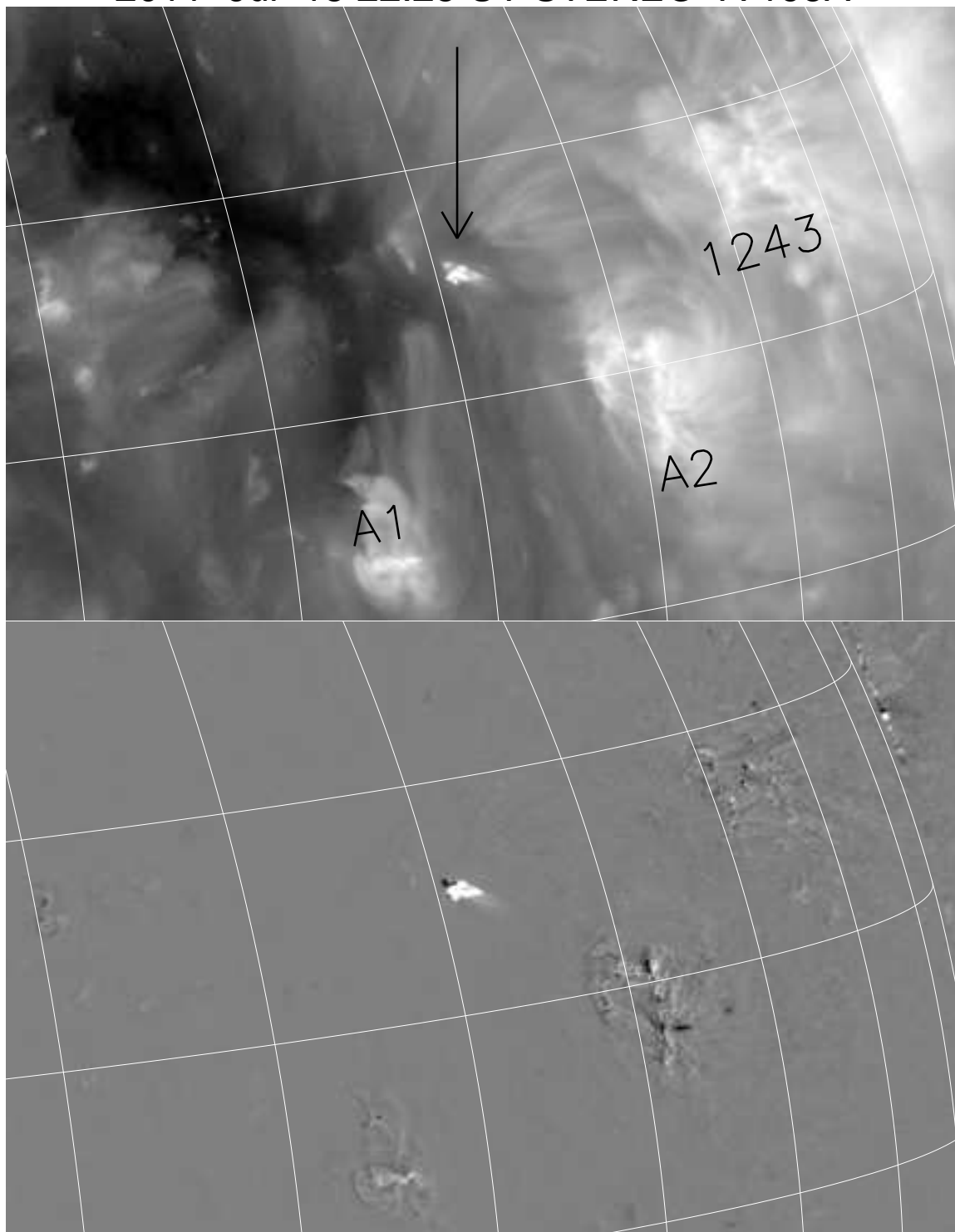


FIG. 9.— *STEREO-A/SECCHI* 195 Å EUV regular (upper panel) and five-minute difference (lower panel) image on 2011 July 15 at 22:25 UT. Marked are regions A1, A2, and AR 11243. The heliographic longitude - latitude grid has 10° spacing. The arrow points to the jet in AR 11246 located at coronal hole border at  $\sim\text{N}15^\circ\text{W}40^\circ$ .

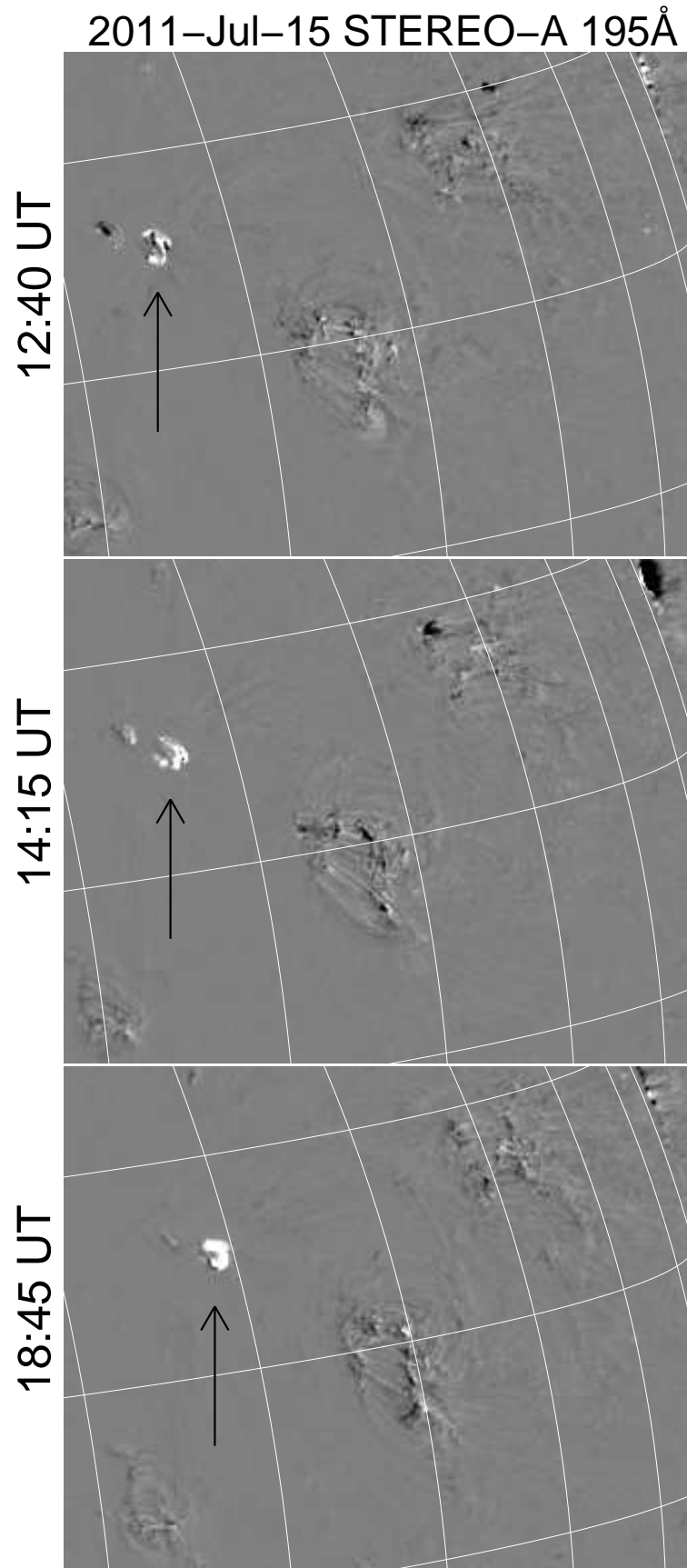


FIG. 10.— *STEREO-A*/SECCHI 195 Å EUV 5-minute difference images on 2011 July 15 at 12:40, 14:15 and 18:45 UT. Arrows point to the brightening in AR 11246 at the western coronal hole border.

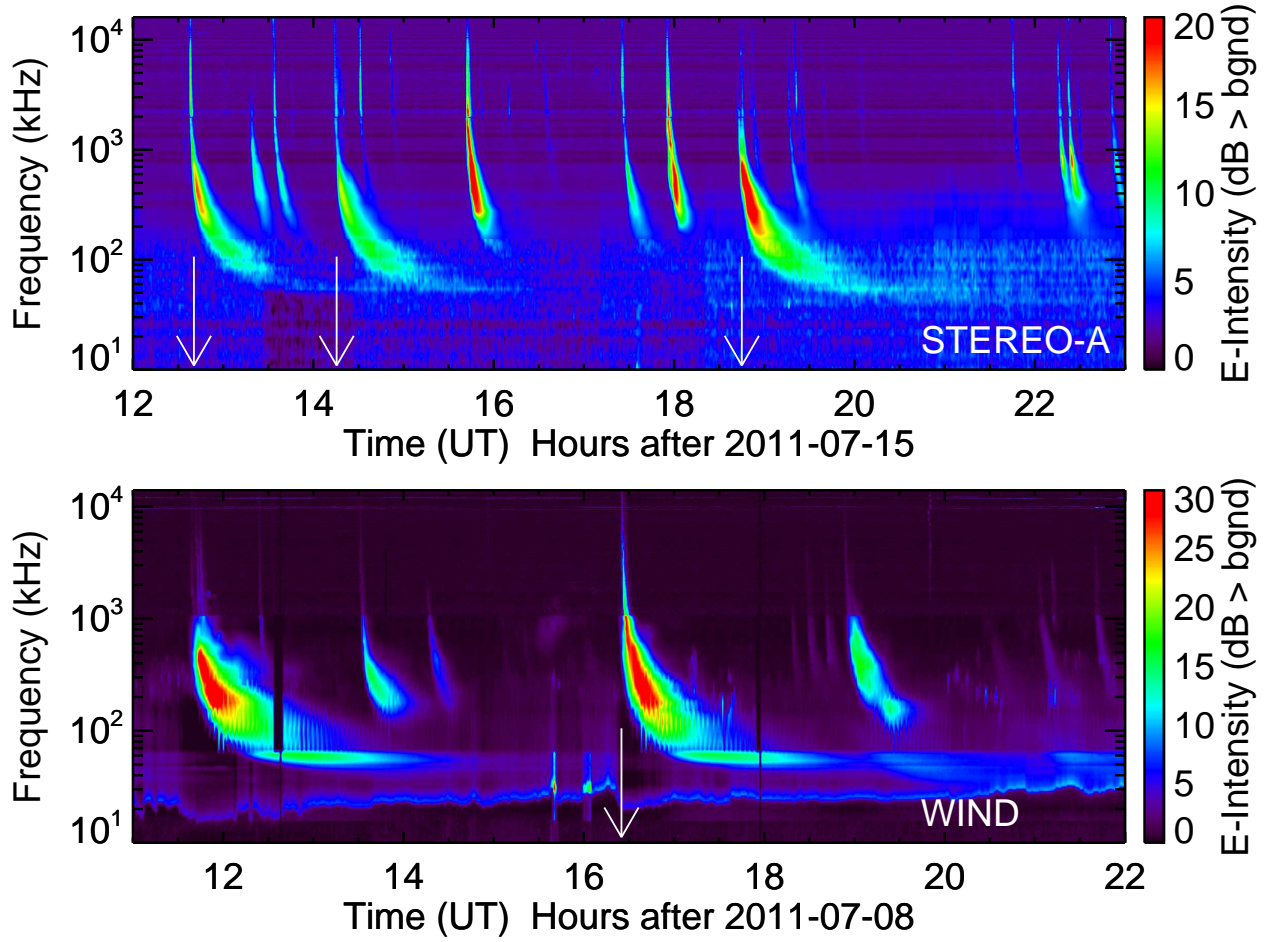


FIG. 11.— Radio spectrogram from *STEREO-A* (upper panel) and *WIND* (lower panel) WAVES instruments. Arrows indicate time of the brightenings and jet in AR 11246.

TABLE 1  
<sup>3</sup>He-RICH PERIOD PROPERTIES

Start Day	2011 Jul 1	2011 Jul 7	2011 Jul 9 <sup>a</sup>	2011 Jul 16 <sup>a,b</sup>
Spacecraft (s/c)	<i>STEREO-B</i>	<i>ACE</i>	<i>ACE</i>	<i>STEREO-A</i>
s/c Carrington Lon. <sup>c</sup>	283°	296°	280°	281°
s/c Heliographic Lat.	-6.9°	3.6°	3.7°	5.0°
<sup>3</sup> He-Rich Interval (doy)	182.9–183.6	188.9–190.0	190.0–191.0	197.5–198.3
<sup>3</sup> He/ <sup>4</sup> He <sup>d</sup>	0.74±0.17	0.42±0.04	2.35±0.13	4.08±0.29
Fe/O <sup>d</sup>	...	0.91±0.15	1.31±0.20	1.19±0.31
<sup>3</sup> He Fluence <sup>d</sup> (×10 <sup>3</sup> )	3.73±0.63	20.6±1.6	127±4	96.1±3.2

<sup>a</sup> event included in survey by Bučík et al. (2013a)

<sup>b</sup> event included in survey by Bučík et al. (2013b)

<sup>c</sup> at event start time

<sup>d</sup> 320-450 keV nucleon<sup>-1</sup>; fluence units - particles (cm<sup>2</sup> sr MeV/nucleon)<sup>-1</sup>